Journal of Nuclear Materials 173 (1990) 185–213
North-Holland

MISTRAL: A COMPREHENSIVE MODEL FOR TRITIUM TRANSPORT IN LITHIUM-BASE CERAMICS
Part I: Theory and description of model capabilities *

G. FEDERICI, A.R. RAFFRAY and M.A. ABDOU

Mechanical, Aerospace, and Nuclear Engineering Department, University of California at Los Angeles, Los Angeles, CA 90024-1597, USA

Received 20 November 1989; accepted 1 May 1990

MISTRAL is a theoretical model developed to describe tritium transport and release in fine-grained ceramic materials for tritium breeding applications in fusion blankets. The model includes as relevant physical processes tritium diffusion in the effective bulk (grains and grain boundaries), adsorption, recombination and desorption at the breeder surface and diffusion through the network of pores. A key improvement of the model, compared with those already in the literature, consists of a better characterization of the processes at the breeder surface and their linking to the bulk and pore regions. The sets of governing transport equations and corresponding boundary conditions are formulated together with the choice of the computational algorithm. A computer code with transient capabilities has been developed based on the model. It aims at describing tritium release for several transient conditions relevant for in-pile tritium recovery experiments and for fusion blankets. To assess the range of applicability of the model, several calculations have been performed and the results of the analysis are herein presented and discussed.

1. Introduction

The processes by which tritium migrates through lithium-base ceramics (e.g. Li_2O, $LiAlO_2$, Li_4SiO_4, Li_2ZrO_3) are complex and of considerable interest for solid breeder blanket components for fusion applications. They determine the rate at which tritium will be released from the breeder material and, consequently, the tritium inventory build-up that results from irradiation in in situ tritium recovery experiments or in fusion reactors. Tritium, which is generated in the candidate breeder materials primarily by the $^6Li(n,\alpha)T$ reaction, is believed to diffuse through the grains to the grain boundaries and, then, along the grain boundaries to the network of interconnected pores. At the solid/gas interface between the effective bulk and the pores, tritium desorbs in molecular form as T_2, HT, T_2O and HTO depending on the chemistry of the solid and gas-phase and then percolates through the network of fine pores to a purge stream which convects the tritium out of the breeder. In materials of interest, the underlying kinetics of the rate-controlling mechanisms of the release are very complex and strongly dependent on the breeder microstructure, the temperature, the purge gas composition and the irradiation history.

In general, tritium release may be diffusion-controlled or constrained by surface processes such as adsorption and desorption. As a ceramic breeder undergoes changes in temperature and/or changes in purge gas composition, it may move from a regime dominated by diffusion to a regime dominated by desorption processes or to a transition regime where both mechanisms control the release. Therefore, to fully interpret the results which are becoming available from in-pile tritium recovery experiments and to understand the synergistic interplay of the several transport processes which take place within the breeder, there is a strong need to develop more comprehensive models and in turn better predictive capabilities. Although much work, both experimental and theoretical, has been reported in the literature on the behavior of hydrogen isotopes in metals [1–4], until very recently few publications existed treating the problem of hydrogen isotope behavior in

* Work supported by the US Department of Energy under grant # DE-FG03-86ER52123.

ceramic breeder materials. Several authors have attempted to outline a theoretical approach to the problem, but no comprehensive theories have emerged yet.

This paper describes the tritium transport model MISTRAL, which has recently been developed to attempt a more realistic and accurate description of the complex multiprocess sequence that characterizes tritium behavior and release in fine-grained lithium-base ceramics. The acronym stands for Model for Investigative Studies of Tritium Release in Lithium Ceramics. The model includes: diffusion through the grain; diffusion along the grain boundaries; adsorption, recombination and desorption at the solid/gas interface; and diffusion along the network of interconnected pores. A key feature of the model covers the kinetics associated with the transfer of tritium generated in the bulk to the surface and from the gas phase onto the surface and vice versa, which are of prime importance in modeling tritium behavior in ceramic breeders and deserve detailed study.

The model development is presented in section 2 including the definition of the geometry and the analytical formulation of the governing transport mechanisms, while section 3 outlines the numerical treatment and the computer code development. More detailed information about the model can be found in ref. [5]. Section 4 presents the results of the calculations carried out to assess the range of applicability and the flexibility of the proposed model. This is followed by the summary section. The comparison of model predictions with results available from in-pile tritium recovery experiments to assess the adequacy of this tritium transport model is presented in Part II of this paper [6]. The symbols and notations are given in a separate nomenclature section.

2. Description of the model

2.1. Modeling background

The most important part in developing a physical model of any sort is the identification of the controlling physical processes and the definition of the differential equations which govern the evolution of the phenomena under investigation. For tritium transport behavior in ceramic breeder materials in a typical fusion environment, the potential number of contribution mechanisms may be very large. The limited amount of experimental data acquired so far leads to the following tentative step description:

1. Production of tritium gas within the grains, primarily by $^{6}Li(n,\alpha)T$ reactions.
2. Migration of atomic tritium to the grain boundaries by intragranular diffusion.
3. Motion of the gas along the grain boundaries to the network of interconnected pores within the solid breeder.
4. Adsorption, desorption and surface reaction of tritium and tritium compounds at the solid/gas interface.
5. Diffusion of tritium and tritium compounds along the interconnected pores and release to the purge flow.
6. Convective transfer out of the breeder by the helium purge stream.

Some tritium beyond that needed for concentration-driven diffusion and desorption will remain in and on the solid breeder because of chemical solubility, precipitation of tritium compounds and radiation-induced trapping. Depending on the specific design of the blanket with regard to coolant, structural material and purge stream, some tritium may also be lost to the coolant stream through permeation.

Which of the above processes are rate limiting for tritium release and contribute the most to the tritium inventory within the solid breeder depend on the operating temperature range, the chemistry of the gas phase, and microstructural parameters, such as grain size, specific surface area and pore size distribution.

Presentation of this modeling analysis needs to be prefaced by showing the features of the model and how it relates to those already in literature.

(A) The model can be classified by the geometry of the effective bulk, surface and pore regions which is used for the physical and mathematical analyses. The selected multiregion, heterogeneous model configuration depicts a more realistic picture of the different morphological regions of the breeder and allows a better description of the transport mechanisms which are effective in the bulk of the solid and gas phases and at the interfaces between solid and gas.

(B) Early tritium release models from ceramic materials were based on the assumption that diffusion in the grain would be rate controlling and only recently an attempt has been made by Kopasz et al. [7] to include a simplified desorption-flux boundary condition to the solution of the diffusion equation in the grains. However, in general, these models were unable to satisfactorily interpret many of the data obtained from in-pile tritium release experiments and their applicability was limited to few particular cases. As yet, no single fundamental method of calculating tritium release exists, the major reasons being: (1) many potentially important variables are involved, the mathematical de-

scription of which may be complex, (2) the data against which the hypothesis can be tested are themselves subject to considerable uncertainties. On the other hand, it is important for the model to properly describe the underlying physics, because fits with physically unsound models to experimental data by adopting suitable parameters will fail whenever extrapolations are needed to new ranges of operating conditions.

(C) Physical processes at the solid/gas interface in ceramic breeder media are currently poorly understood and their modeling is limited. In fact, many of the existing models assume an effective bulk diffusion with or without a desorption flux boundary condition at the breeder surface where the concentration of the diffusing substance is obtained by neglecting any kind of transport mechanisms into the solid from the surrounding gas phase. In contrast, in several experiments the characteristics of the purge gas, such as its composition and flow rate, have been identified as crucial factors clearly indicating that the phase-boundary region between the solid and the gas may strongly affect the overall kinetics of the release. This capability has been incorporated in this model which focuses on the kinetics associated with transport processes at the breeder surface, such as adsorption and desorption.

(D) Contrary to previous mathematical models, which can be applied to analyze transient conditions limited to changes in temperature, MISTRAL has a greater flexibility and is able to analyze several transient conditions such as changes in temperature and temperature gradient, changes in purge gas composition, and changes in reactor power (i.e. neutron flux), all foreseen in a fusion blanket operation.

(E) As a final remark, the numerical algorithm selected to solve the governing partial differential equations in the present model is particularly suitable for parametric analysis. It can be applied to determine functional dependence and also to provide insight into the interrelationships of the various operating conditions and material properties which may affect the behavior of tritium in the material.

2.2. Definition of the model geometry

The model proposed in this work is based on the concept of interconnected and open porosity, which is perhaps the simplest model for diffusion and flow in a porous solid. The occurrence of interconnected pores represents a realistic condition for the structure of the ceramic breeder. In this case, it is not the total porosity but the open interconnected porosity which is the key parameter that needs to be characterized for the ceramic breeder before, during and after the reactor operation. According to the indications provided by Elbel [8], for as-fabricated cases, the amount of open porosity can be substantial, in particular for cases with high total porosity, ranging between 80–100% of the total porosity. The pores can then be represented as interconnected cylindrical capillaries having some effective radius and length. To account for the shape and orientation of pores in the real geometry, an adjustable constant, the tortuosity δ, is included. Although ceramic grains are irregular polyhedrons, for ease of calculation the model is presumed to be composed of spherical grains. More detailed structural models have been proposed by Wheeler [9] and by Wakao et al. [10], but often these are of such complexity that they become difficult to validate and to use conveniently.

The unit cell in the model has been identified as the cylindrical portion of the solid that surrounds each

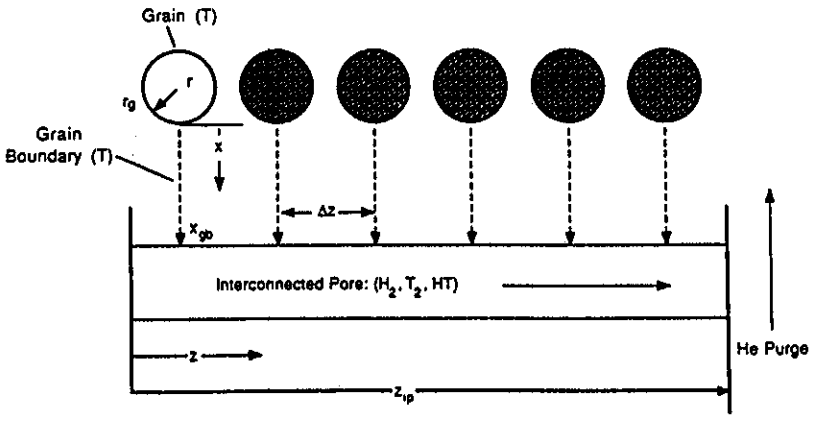

Fig. 1. Schematic diagram of the multiregion model.

interconnected channel and it is characterized by: (1) a cylindrical interconnected pore of effective length, L_e, and average radius, r_{ip}; (2) a coaxial cylindrical cluster of spherical grains of radius, r_g. A schematic diagram of the multiregion model is shown in fig. 1. In general, the quantities that are known are the solid breeder specimen characteristic length, L, the average grain radius, r_g, the specific surface area, S_{BET} (after Brunauer, Emmett and Teller [12]), the theoretical density of the solid, ρ, and the porosity, ϵ_p. The effective length L_e for the interconnected pore channel has been defined by Youngquist [11] in terms of the characteristic length of the specimen as follows:

$$(L_e/L)^2 = \delta, \tag{1}$$

where, δ is the tortuosity factor. δ can be estimated from $1/\epsilon_p$ for as-fabricated breeder materials based on the model of Wakao et al. [10]. However, the tortuosity factor can be much higher as indicated by the experimental data of Krasuk et al. [13] for example, although it is not always clear how to differentiate between the effect of longer diffusion path and of slower effective diffusion due to the pore size distribution. These are often combined when expressing the tortuosity factor as indicated by Satterfield [14].

$$L_e = L\sqrt{\delta}\,. \tag{2}$$

An estimate of the average pore size, r_{ip}, may be obtained from the void volume-surface area formula suggested by Aris [15]:

$$r_{ip} = \frac{2\epsilon_p}{\rho(1-\epsilon_p)S_{BET}}. \tag{3}$$

Once the average pore radius r_{ip} has been determined, the number of grains per interconnected pore system, N_{gip}, can be derived from the following expression [5]:

$$N_{gip} = \frac{2\pi r_{ip} L_e}{S_{BET}\rho V_g}. \tag{4}$$

The volume V_{ip} of each interconnected pore system may then be expressed as:

$$V_{ip} = \pi r_{ip}^2 L_e. \tag{5}$$

The total number of interconnected pore systems (i.e. unit cells) in the specimen of volume V is given as:

$$N_{ip} = V\epsilon_p/V_{ip}. \tag{6}$$

The shape of the cross section of the unit cell is determined by the average radius of the grain and the average radius of the interconnected pore, and it may be represented by a regular polygon of a certain number of sides, N_{sides}, that has to be determined by simple geometrical considerations.

The vertex angle, Θ, (radians) can be evaluated as:

$$\Theta = \pi\left(\frac{N_{sides}-2}{N_{sides}}\right). \tag{7}$$

The number of grain boundary paths per grain, N_{gbg}, is calculated from:

$$N_{gbg} = 4\pi/\Theta. \tag{8}$$

The number of grains per grain boundary path, N_{ggb}, is given by:

$$N_{ggb} = 1/N_{gbg}. \tag{9}$$

According to the model, the grain boundary path length is the average distance the gas will migrate on the grain surface before desorbing to the pore and it may be defined on the basis of geometrical considerations as:

$$x_{gb} = \frac{r_g}{6}(\Theta + \pi), \tag{10}$$

where a factor of 1/3 was introduced to average over the path length. For a grain boundary of thickness t_{gb}, the volume of each grain boundary path, V_{gb}, is:

$$V_{gb} = r_g^2 \Theta t_{gb}/2. \tag{11}$$

Finally, approximating V_{gb} as a slab of transversal area A_{gb} and average length x_{gb} yields:

$$A_{gb} = V_{gb}/x_{gb}. \tag{12}$$

2.3. Theoretical treatment of tritium transport in solid breeder media

A system of differential equations governing the space and time evolution of tritium in each morphological region of the breeder, such as grain, grain boundary, surface and pore has been derived. The equations that describe the behavior of the gas are essentially diffusion equations in the breeder bulk and along the network of interconnected pores and rate equations that govern the transport at the interfaces between different phases. An adequate set of boundary conditions has been proposed to correctly couple the individual transport processes in each morphological region of the breeder.

2.3.1. Diffusion in the grains

Individual grains are assumed to be discrete, homogeneous, isothermal spherical particles. Tritium is assumed to be uniformly generated by breeding reactions in the grains and at this stage the atoms are assumed to be completely insoluble in the matrix. Grain sizes are

typically of the order of microns and each grain can reasonably be assumed to be isothermal.

The governing diffusion equation for the concentration of gas atoms C_g in the grain may then be written as:

$$\frac{\partial C_g(r,t)}{\partial t} = D_g(T)\left[\frac{\partial^2 C_g(r,t)}{\partial r^2} + \frac{2}{r}\frac{\partial C_g(r,t)}{\partial r}\right] + \mathscr{G}(t), \tag{13}$$

where $C_g(r, t)$ is the tritium concentration within the grain, at spatial coordinate r and time t, $D_g(T)$ is the tritium diffusion coefficient in the grain as a function of the temperature T, $\mathscr{G}(t)$ is the volumetric tritium generation rate in the grain at spatial coordinate r and time t, and r_g is the grain radius.

The diffusivity in the grain is given by an Arrhenius function as:

$$D_g(T) = D_{g0}\exp\left[-E_g(T)/RT\right], \tag{14}$$

where D_{g0} is the pre-exponential factor for diffusion in the grain, $E_g(T)$ is the activation energy for diffusion in the grain and is a function of the temperature T, and R is the universal gas constant.

The boundary conditions assumed for the grain are:

(a) symmetry condition at the center of the grain:

$$\left[\frac{\partial C_g(r,t)}{\partial r}\right]_{r=0} = 0, \tag{15}$$

(b) continuity of the concentration at the boundary between grain and grain boundary:

$$V_g C_g(r_g, t) = V_{gbg} C_{gb}(0, t), \tag{16}$$

where $C_g(r_g, t)$ is the grain concentration at the grain surface, $C_{gb}(0, t)$ is the concentration at the grain boundary/grain interface (i.e., at the beginning of the equivalent grain boundary path in the shape of a slab). V_g is the volume of each grain and $V_{gbg}(= V_{gb}N_{gbg})$ is the equivalent grain boundary volume associated with each spherical grain. The factor V_g/V_{gbg} in eq. (16) is introduced to account for the particular geometry of the model.

2.3.2. Diffusion along the grain boundaries

In the proposed model the grain boundaries are supposed to prevent intergrain communication and to be high-diffusivity pathways which are fed by lattice diffusion from the grain interior. In this study, grain boundary diffusion is believed to be much faster than grain diffusion and is not considered to be rate controlling. Mathematical treatment of grain boundary diffusion is included in the model to provide flexibility for later applications. The grain boundary is represented as a uniform, isotropic pathway in the shape of a slab of average thickness t_{gb}, average length x_{gb} and average cross section A_{gb}, within which diffusion occurs in accordance with Fick's law but at a rate different from the bulk. Several authors [16–18] agree that the thickness of the grain boundary t_{gb} is much smaller than any other dimension of the system and that in a domain only a few atoms thick it is reasonable to neglect lateral concentration gradients. In addition, the grain boundary dimensions are of the order of the grain dimensions and, thus, the grain boundary path can be assumed to be isothermal. With these assumptions, the one-dimensional time-dependent diffusion equation for the grain boundary then becomes:

$$\frac{\partial C_{gb}(x,t)}{\partial t} = D_{gb}(T)\left[\frac{\partial^2 C_{gb}(x,t)}{\partial x^2}\right], \tag{17}$$

where $C_{gb}(x, t)$ is the tritium concentration within the grain boundary, at spatial coordinate x and time t, $D_{gb}(T)$ is the tritium diffusion coefficient in the grain boundary as a function of the temperature T, and x_{gb} is the average grain boundary length. The diffusivity in the grain boundary is given by an Arrhenius function as:

$$D_{gb}(T) = D_{gb0}\exp\left[-E_{gb}(T)/RT\right], \tag{18}$$

where D_{gb0} is the pre-exponential factor for diffusion along the grain boundary, and $E_{gb}(T)$ is the activation energy for grain boundary diffusion and is a function of the temperature T.

The following boundary conditions are assumed for the grain boundary region:

(a) flux-matching condition at the interface between grain boundary and grain:

$$4\pi r_g^2 N_{ggb} D_g(T)\left[\frac{\partial C_g(r,t)}{\partial r}\right]_{r=r_g} = A_{gb} D_{gb}(T)\left[\frac{\partial C_{gb}(x,t)}{\partial x}\right]_{x=0}, \tag{19}$$

where N_{ggb} and A_{gb} represent the number of grains per grain boundary and the equivalent grain boundary transversal area, respectively. The factor $4\pi r_g^2$ represents the surface of the grain.

(b) flux-matching condition at the effective bulk and phase boundary interface:

$$D_{gb}(T)\left[\frac{\partial C_{gb}}{\partial x}\right]_{x=x_{gb}} = \beta_0\exp\left[-E_\beta/RT\right](1-\theta)C_{gb}(x_{gb}, t). \tag{20}$$

The tritium concentration $C_{gb}(x_{gb}, t)$ in the effective bulk region just beneath the surface is determined by the adsorption/desorption processes as shown in the previous equation, where the right-hand term represents the rate of filling of surface adsorption sites by tritium atoms. In eq. (20), θ is the total coverage and β_0 is the pre-exponential factor proposed by Pick [19] $\approx 1 \times 10^{13}/\sqrt{N_S}$ (m/s), where N_S is the density of surface sites.

2.3.3. Treatment of surface processes

After migrating along the grain boundary paths, tritium reaches the solid/gas interface where it desorbs into the pore, in combination with any oxygen or hydrogen present at the surface.

Adsorption and desorption of gases onto surfaces, as well as surface reactions of the adsorbed species, are complicated phenomena, and their modeling can be built with various levels of sophistication. The model presented here is based on the idealized potential energy diagram at the surface shown in fig. 2. The solid surface is assumed to be covered with a number of sites at which atoms of the adsorbate may be held. The forces which hold them there are either physical, such as van der Waals' attraction, or chemical, in which the adsorbate–adsorbent bond approaches an ordinary bond in strength and in which the chemical nature of the adsorbate may be significantly different in the adsorbed state. Such adsorption is generally called chemisorption, to distinguish from the former, which is called physisorption.

In tritium release experiments, what is regarded as the desorption step really involves two processes: (1) a surface reaction between tritium and chemisorbed hydrogen to form surface bound HT or HTO, and (2)

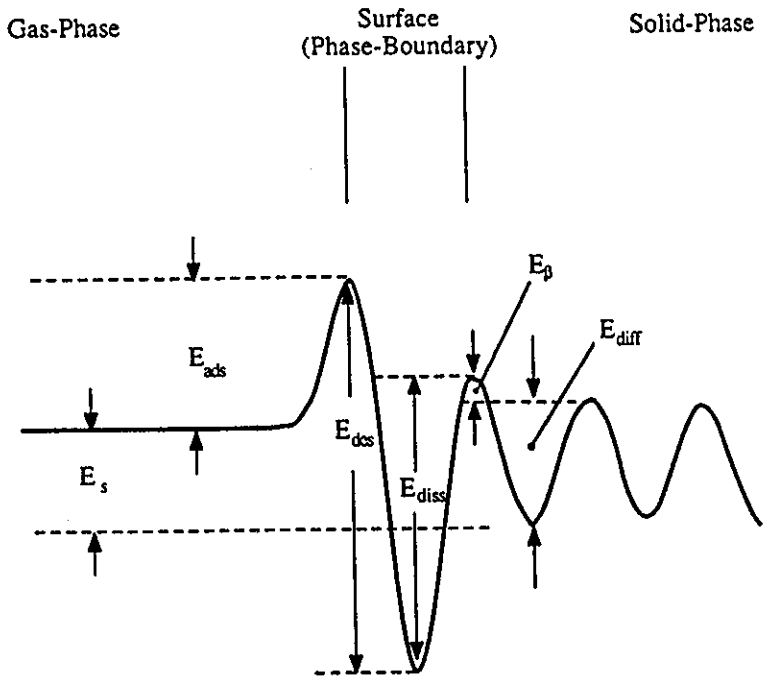

E_{ads} = Activation Energy for Adsorption
E_β = Activation Energy for Adsorption from the Bulk
E_{des} = Activation Energy for Desorption
E_{diss} = Activation Energy for Entering the Bulk
E_{diff} = Activation Energy for Bulk Diffusion
E_s = Solution Energy

Fig. 2. Potential energy diagram for hydrogen isotopes at the surface used in the model.

desorption of the surface bound HT or HTO. These processes can be expressed as

$T_{(s)} + H_{(s)} \rightarrow HT_{(s)}$.

$T_{(s)} + OH_{(s)} \rightarrow HTO_{(s)}$.

$HT_{(s)} \rightarrow HT_{(g)}$.

$HTO_{(s)} \rightarrow HTO_{(g)}$.

where the suffix (s) represents a surface bound state and the suffix (g) represents a species in the gas phase. The activation energies of either the surface reactions or the actual desorption of the surface bound atoms may be strongly dependent on the surface coverage. In the model to describe the kinetics of adsorption and desorption of tritium-bearing species, the fluxes of tritium atoms from the bulk to the surface and the fluxes of molecules from the pore to the surface and from the surface to the pore must be included. A rate theory formulation has been used to model surface phenomena and the details of the scheme adopted in the model are hereafter outlined.

At this stage, the model assumes that the hydrogen in the pore are either completely in their reduced states or completely in their oxidized states. Thus, in the following equations (i) could refer to species HT, T_2 or H_2 in the former case, or to species HTO, T_2O and H_2O in the latter case. The (j) notation, instead, refers to the individual H and T atoms irrespective of their chemical states.

The following fluxes to and from the surface are included in the surface model represented in fig. 3.

(1) Flux of tritium atoms (atoms/m^2 s) entering the surface from the bulk side. This flux can be formulated with an expression similar to that used by Pick in ref. [19]:

$$\Re_1^T = k_\beta(T) C_{gb}(x_{gb}, t)(1-\theta), \tag{21}$$

where $C_{gb}(x_{gb}, t)$ is the tritium concentration just beneath the surface at time t, $\theta^{(j)}$ is the fractional coverage for the adsorbed species (j), θ is the total coverage, $\theta = \sum_{j=1}^{N} \theta^{(j)}$, $(1-\theta)$ is the fraction of sites available and the rate constant $k_\beta(T)$, a function of the temperature, can be expressed as:

$$k_\beta(T) = \beta_0 \exp\left[-E_\beta/RT\right], \tag{22}$$

where E_β is the activation energy for adsorption from the bulk, and β_0 is the pre-exponential factor proposed by Pick [19] $\approx 1 \times 10^{13}/\sqrt{N_S}$.

(2) Flux of diatomic molecules of species (i) (molecules/m^2 s) entering the surface from the pore-side. Each molecule strikes the surface, dissociates and is adsorbed as two atoms:

$$\Re_2^{(i)} = k_{ads}^{(i)}(T, \theta) C_p^{(i)}(z, t)(1-\theta)^2, \tag{23}$$

where $C_p^{(i)}(z, t)$ is the concentration of the gas species (i) along the pore at spatial coordinate z and time t,

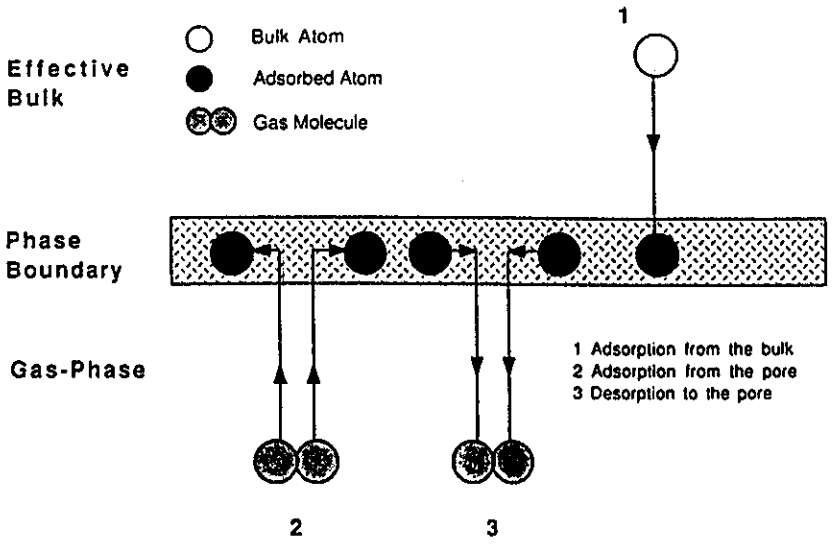

Fig. 3. Schematic of the surface processes included in the model.

and the rate constant $k_{ads}^{(i)}(T, \theta)$ for dissociative adsorption is given by Boudart et al. [20] as:

$$k_{ads}^{(i)}(T, \theta) = \frac{\sigma N_z}{\sqrt{8 \times 10^{-3} \pi}} \sqrt{\frac{RT}{M^{(i)}}} \times \exp(-E_{ads}(T, \theta)/RT), \quad (24)$$

where $E_{ads}(T, \theta)$ is the activation energy for adsorption from the pore, as a function of the temperature and of the degree of coverage. σ is the condensation or trapping coefficient, (usually $\sigma \approx 0.4$), N_z is the number of adjacent sites (usually $N_z = 4$), R is the universal gas constant, T the absolute temperature and $M^{(i)}$ molecular weight of species (i).

(3) A pair of adsorbed atoms of species (j) and (q) (with corresponding coverages $\theta^{(j)}$ and $\theta^{(q)}$) combines and desorbs as a molecule of species (i), (molecules/m^2 s):

$$\Re_3^{(i)} = k_{des}(T, \theta)\theta^{(q)}\theta^{(j)}, \quad (25)$$

where the rate constant $k_{des}(T, \theta)$ for associative desorption is given by Boudart et al. [20] as:

$$k_{des}(T, \theta) \approx \tfrac{1}{2} N_z \frac{RTN_S}{N_{avo}h} \exp(-E_{des}(T, \theta)/RT), \quad (26)$$

where $E_{des}(T, \theta)$ is the activation energy for associative desorption as a function of coverage, h is Planck's constant, R is the Universal gas constant, N_{avo} is Avogadro's number, N_S is the density of surface sites and N_z is the number of adjacent sites.

It is important to realize that it is the surface coverage θ which determines the flux from the surface and not the concentration in the bulk, and that the surface coverage can differ considerably from the bulk concentration.

Generally, the surface barrier model proposed by Pick et al. [21,22] includes also a flux of atoms leaving the surface and entering the bulk. Indeed, a complicating factor with all adsorption studies arises from the fact that adsorbed tritium and hydrogen atoms on the surface may penetrate the phase boundary into the bulk. A typical reaction scheme for the interaction of hydrogen with a metal was formulated by Wagner [23] about fifty years ago as follows:

$$H_{2,(gas)} + 2* \rightleftharpoons 2H_{ads},$$

$$H_{ads} \rightleftharpoons H_{bu} + *,$$

H_{bu} denotes a hydrogen atom in the bulk. H_{ads} is the (atomic) chemisorbed state and $*$ a free adsorption site.

(4) According to the previous reaction scheme, this dissolution flux of adsorbed atom entering the bulk (atoms/m^2 s) can then be characterized as:

$$\Re_4^{(j)} = k_{diss}(T)\theta^{(j)}, \quad (27)$$

where the rate constant $k_{diss}(T)$ as a function of the temperature can be expressed as:

$$k_{diss}(T) = \alpha_0 \exp[-E_{diss}/RT]. \quad (28)$$

α_0 is the pre-exponential factor and E_{diss} is the activation energy for atomic dissolution into the bulk.

Balancing the adsorption fluxes at the surface (phase boundary) from the pore and from the bulk regions with the desorption flux into the pore and the dissolution flux into the bulk, yields the following system of rate equations governing the coverage for each adsorbed species (j):

$$\frac{d(N_S\theta^{(j)})}{dt} = \Re_1^T + \sum_{(i)} \gamma_{(i)}^{(j)} \Re_2^{(i)} - \sum_{(i)} \gamma_{(i)}^{(j)} \Re_3^{(i)} - \Re_4^{(j)}, \quad (29)$$

where $\gamma_{(i)}^{(j)}$ is number of atoms of species (j) which adsorbs or desorbs per each gas molecule of species (i). In eq. (29), $\Re_1^T = 0$ for (j) = hydrogen.

However, in this study the main emphasis is directed towards the adsorption and desorption processes and is assumed that a negligible bulk uptake occurs (i.e., $\Re_4^{(j)} \rightarrow 0$). Moreover, other surface processes, conceptually possible proposed by Baskes [24] and by Richards [25], such as direct desorption from the bulk to the gas with or without pausing and recombining on the phase boundary, or direct dissolution into the bulk of atoms coming from the pore, and which may be easily incorporated in the proposed surface model, are ignored in this analysis for ease of calculation.

Therefore, neglecting dissolution into the bulk and inserting the proposed expressions for the fluxes $\Re_1^T$, $\Re_2^{(i)}$ and $\Re_3^{(i)}$ results in:

$$\frac{d[N_S\theta(z, t)^{(j)}]}{dt} = k_\beta(T)C_{gb}(x_{gb}, t)[1 - \theta(z, t)] + \sum_{(i)} \gamma_{(i)}^{(j)} k_{ads}^{(i)}(T, \theta)C_p^{(i)}(z, t)[1 - \theta(z, t)]^2 - \sum_{(q)} \gamma_{(q)}^{(j)} k_{des}(T, \theta)\theta(z, t)^{(q)}\theta(z, t)^{(j)}, \quad (30)$$

where the summations include all the gas species (i) in the gas phase and all the species (q) adsorbed on the surface. The factor $\gamma_{(i)}^{(j)}$ represents the number of atoms of species (j) adsorbed per molecule of species (i) while the factor $\gamma_{(q)}^{(j)}$ represents the number of atoms of

species (j) that desorb after recombining with any atom of species (q).

2.3.4. Diffusion equations through interconnected pores

In the interconnected pore system the flux of each gas species should depend on the gradients of all the other species and of temperature. Therefore, by neglecting radial gradients, the following one-dimensional diffusion equation is used for determining the concentration of each gas species (i) along the interconnected pore:

$$\frac{\partial C_p^{(i)}(z,t)}{\partial t} = \frac{\partial}{\partial z}\left[D_{p_{eff}}^{(i)}(T)\frac{\partial C_p^{(i)}(z,t)}{\partial z}\right] + \mathscr{G}_p^{(i)}(z,t), \tag{31}$$

where $C_p^{(i)}(z,t)$ is the concentration of molecules of species (i) along the pore at spatial coordinate z and time t, $D_{p_{eff}}^{(i)}(T)$ is the effective pore diffusion coefficient for species (i) as a function of temperature T. $\mathscr{G}_p^{(i)}(z,t)$ is the volumetric source/sink term for species (i) in the pore at spatial coordinate z and time t, and z_{ip} is length of the interconnected pore system and is equal to the effective pore length, L_e defined by eq. (2). Note that the behavior of helium in the pore is neglected under the assumption that the concentration or partial pressure of helium is much larger than that of the tritium and/or hydrogen gas species and that the helium in the pore is stagnant. The following boundary conditions are assumed for the pore region:

(a) zero gradient for each species (i) at the beginning of the interconnected pore (i.e., no diffusion flux at $z = 0$):

$$\left[\frac{\partial C_p^{(i)}(z,t)}{\partial z}\right]_{z=0} = 0, \tag{32}$$

(b) given concentration for each species (i) at the end of the interconnected pore system ($z = z_{ip}$):

$$C_p^{(i)}(z_{ip},t) = C_{purge}^{(i)}. \tag{33}$$

Diffusion of a gas in a porous medium is complicated by the fact that different diffusion mechanisms may in effect depend on the structure of the porous material. According to Youngquist [11], three different regimes are possible, namely, (1) ordinary diffusion in which molecular collisions dominate the diffusion process, (2) Knudsen diffusion in which collisions of the diffusing molecules with the porous solid dominate the diffusion process, and (3) a transition region between the above two diffusion regimes. Which regimes is in effect depends on the ratio of the mean-free-path of the diffusing species, λ, to the characteristic pore radius, r_{ip}. A value of $\lambda/r_{ip} \le 0.10$ results in ordinary diffusion, while $\lambda/r_{ip} \ge 10.0$ results in Knudsen diffusion, and $0.10 \le \lambda/r_{ip} \le 10.0$ results in transition region diffusion.

To estimate the applicable regime, the mean-free-path, λ, and the representative channel radius, r_{ip}, must be estimated. An estimate of r_{ip} is given by eq. (3), while the mean-free-path (in meters) can be obtained from the following expression:

$$\lambda_{i,l} = \frac{k_B T}{\sqrt{2}\,\pi\sigma_{i,l}^2 p}, \tag{34}$$

where k_B is Boltzmann's constant, $\sigma_{i,l}$ is the constant in the Lennard–Jones [26] potential energy function for the molecular pair (i, l) (here $\sigma_{i,l}$ is in meters) and p is the gas pressure in Pascals.

For flow of binary mixtures (i, l) in a single capillary (which is often employed to represent flow in a porous medium), the Knudsen diffusion coefficient, $D_K^{(i)}$, is given by:

$$D_K^{(i)}(T) = \tfrac{2}{3} r_{ip}\sqrt{\frac{8RT}{\pi M^{(i)}}}. \tag{35}$$

Note that in this case the rate of diffusion of species (i) is independent of component (l) and is proportional to the capillary radius r_{ip}.

For ordinary diffusion at low pressure, the Chapman–Enskog formula for the diffusion coefficient, $D_o^{(i)}$, given by Bird et al. [27] can be employed, namely,

$$D_o^{(i)}(T) = 1.8583\times 10^{-7}\frac{T^{3/2}\sqrt{1/M^{(i)} + 1/M^{(l)}}}{p\sigma_{i,l}\Omega_{i,l}}, \tag{36}$$

where in eq. (36) T is the absolute temperature in K, $M^{(i)}$, $M^{(l)}$ are the molecular weights of gas (i) and (j), p (atm) is the total pressure of the gas mixture, $\sigma_{i,l}$ is the constant in the Lennard–Jones potential-energy function for the molecular pair (i, l) (here, $\sigma_{i,l}$ in Å), and $\Omega_{i,l}$ is the collision integral.

Finally, for the transition region, the expression for the transition coefficient, $D_T^{(i)}$ derived by Youngquist [11] is proposed

$$D_T^{(i)}(T) = 1/\left[\frac{1-\alpha\mathscr{N}_{(i)}}{D_o^{(i)}(T)} + \frac{1}{D_K^{(i)}(T)}\right], \tag{37}$$

where $\mathscr{N}_{(i)}$ is the mole fraction of species (i) and where

$$\alpha = 1 - \sqrt{M^{(i)}/M^{(l)}}. \tag{38}$$

The pore diffusion coefficient, $D_p^{(i)}(T)$ for flow within an individual capillary is then calculated from eqs. (35)–(37) depending on the diffusion regime. However, the effective diffusion coefficient in the pore, $D_{p_{eff}}^{(i)}(T)$,

can be substantially different from $D_p^{(i)}(T)$. For example, for cases where there is a wide distribution of pore sizes, the effect of a series of constrictions and expansions can significantly lower $D_p^{(i)}(T)$. In addition, if diffusion occurs at least partially in the Knudsen regime, the effective diffusion coefficient can be lower than that based on the average pore radius of eq. (3). Because of these uncertainties regarding the value of D_p, a factor f_{DP} is introduced to enable the analysis of the effect of varying the pore diffusion coefficient on the tritium release behavior.

$$D_{P_{eff}}^{(i)}(T) = f_{DP} D_p^{(i)}(T). \tag{39}$$

The source/sink term $\mathscr{G}_p^{(i)}$ for the species (i) in the pore system, that appears in eq. (31), may be expressed in terms of the rate of adsorption from the pore on the phase boundary $\Re_2^{(i)}$, and the rate of desorption into the pore $\Re_3^{(i)}$ according to the following expression:

$$\mathscr{G}_p^{(i)} = 2\left[\Re_3^{(i)}(T, \theta) - \Re_2^{(i)}(T, \theta)\right]\omega_1. \tag{40}$$

The factor $2\omega_1$ in eq. (40) is introduced to convert fluxes of atoms at the surface in volumetric source into the pore and the constant ω_1 may be defined as:

$$\omega_1 = \frac{N_S S_{BET} \rho V_g N_{gip}}{2V_{ip}}. \tag{41}$$

2.3.5. Effect of reactions in gas phase

In many experiments such as TRIO [28], MOZART [29] and VOM-23 [30] addition of small quantities of hydrogen to the helium purge (up to about 1% by volume of hydrogen) was found to substantially enhance the tritium release. In this study, special effort has been addressed to model the effect of hydrogen in the system and to interpret the experimental data available.

Adding hydrogen (protium) to the purge results in a build-up of hydrogen partial pressure in the network of pores, and in an increase of the adsorption flux of hydrogen-bearing species on the surface. As a result of the competition for active sites at the surface, hydrogen (which is generally present in a much larger quantity than tritium) basically replaces the tritium collected on the surfaces, whose coverage decreases. This effect is known as swamping.

The available data at this stage are not sufficient to describe the kinetics of the chemical reactions in the pore. Therefore, the approach to modeling the gas phase pore chemistry is to assume that the reactions among the hydrogenic species are fast enough for chemical equilibrium to be maintained. In this respect, the surface may act as a catalyst and therefore play a crucial role in the kinetics of these reactions.

The reaction scheme proposed is then:

$$(H_2 - X) + (T_2 - X) \rightleftharpoons 2(HT - X). \tag{42}$$

where in the reduced state X vanishes and in the oxidized state X represents oxygen. Then, assuming local chemical equilibrium for the system under consideration (interconnected pore with H and T-bearing species), one can calculate the final concentrations of H_2 (H_2O), T_2 (T_2O) and HT (HTO) in the pores from the following relationships:

$$\frac{\left[C_p^{(HT-X)}\right]^2}{C_p^{(T_2-X)} C_p^{(H_2-X)}}$$

$$= \begin{cases} K_{eq}(1) & \text{for reduced states,} \quad (43) \\ K_{eq}(2) & \text{for oxidized states.} \quad (44) \end{cases}$$

The model can describe any of the species T_2, H_2 and HT or the species T_2O, H_2O and HTO under the assumption that for the latter any kind of oxygen activity is neglected (i.e., all oxygen present in the pore system is assumed to be combined with hydrogenic species). The equilibrium constants, $K_{eq}(1)$ and $K_{eq}(2)$, are temperature dependent with an approximate value of 4. Values of $K_{eq}(1)$ in the gas phase used here are based on those calculated for different temperatures by Jones [31].

2.3.6. Characterization of the tritium release

At each time-step the release of tritium is expressed in terms of the gradient of the concentrations of the tritium-bearing species in the system calculated at the end of the interconnected pore system for the different tritium concentration species as follows:

$$\mathscr{R} = \frac{\pi r_{ip}^2}{N_{gip}} - \sum_{\substack{\text{T containing} \\ \text{species } (i)}} D_{P_{eff}}^{(i)} \left[\frac{\partial C_p^{(i)}(z, t)}{\partial z}\right]_{z=L_e} \gamma_{(i)}^{(T)}, \tag{45}$$

where $\gamma_{(i)}^{(T)}$ is number of tritium atoms per gas molecule of species (i).

A normalized formulation for the tritium release rate is obtained by dividing, at each time-step, the above expression with the tritium generation rate in the solid breeder volume associated with one interconnected pore system which represents the unit cell in the model.

$$\Re_n = \frac{\pi r_{ip}^2}{\mathscr{G}_{max} V_g N_{gip}} \times \sum_{\substack{\text{T containing} \\ \text{species } (i)}} D_{P_{eff}}^{(i)} \left[\frac{\partial C_p^{(i)}(z, t)}{\partial z}\right]_{z=L_e} \gamma_{(i)}^{(T)}. \tag{46}$$

2.3.7. Characterization of the inventory components in the different regions of the model

The concentration of each gas species at each time-step, as well as its location (within the grains, within the grain boundaries, onto the breeder surface or within the interconnected pore), are of particular interest in gas release and inventory studies. These quantities are of further value in that, when summed to obtain the total mass of gas within the unit cell at various times, an account is kept of how well mass is conserved through the course of the computations (including transport across the system boundaries).

The tritium inventory components, in the different morphological regions of the breeder may be defined as follows:

– *Tritium inventory in one grain*:

$$I_g(t) = 4\pi \int_0^{r_g} C_g(r, t) r^2 \, dr. \tag{47}$$

– *Tritium inventory in the grain boundary (normalized to one grain)*:

$$I_{gb}(t) = A_{gb} N_{gbg} \int_0^{x_{gb}} C_{gb}(x, t) \, dx. \tag{48}$$

– *Tritium inventory on the surface (normalized to one grain)*:

$$I_{surf}(t) = S_{BET} \rho N_S V_g \theta^T. \tag{49}$$

– *Tritium inventory through the interconnected pore (normalized to one grain)*:

$$I_{ip}(t) = \frac{\pi r_{ip}^2}{N_{gip}} \gamma_{(i)}^{(T)} \int_0^{L_e} \sum_{\substack{\text{T containing} \\ \text{species } (i)}} C_p^{(i)}(z, t) \, dz \tag{50}$$

2.4. Summary of the main modeling assumptions

Because of the complexity of the tritium transport phenomena which take place in solid breeders under irradiation, some suitable simplifying assumptions have been introduced in the theoretical model development as follows.

1. Although solid breeder grains are irregular polyhedrons, they are assumed to be spherical for ease of calculation.
2. Elongated interconnected pores are assumed across the solid breeder. Their occurrence is important because they provide an easy path for tritium release.
3. Uniform generation of tritium throughout the solid breeder grain.
4. The grain boundaries shut off intergrain communication.
5. The grain boundaries are assumed to be very high diffusivity paths which are fed by lattice diffusion from the grain interior. In this stage of the model development, the results of the calculations carried out using this model have been obtained by using a value of D_{gb} much higher than D_g. By modifying the grain boundary diffusion coefficient the model can account for transport retardation by grain boundaries as well as enhanced diffusion.
6. The thickness of the grain boundary, t_{gb}, is much smaller than any other dimension of the system. Consequently, no attempt is made to model diffusion perpendicular to the grain boundary.
7. A simplified barrier model is incorporated to model tritium surface processes. The dissolution flux of atoms entering the bulk from the surface has been assumed negligible.
8. Second order or associative desorption and dissociative adsorption are assumed to occur at the surface.
9. No oxygen activity effect has been included (i.e., all oxygen present in the pore system is assumed to be combined with hydrogenic species).
10. No radiation-induced trapping within the grain.
11. No tritium retention within the pore because of sintering and consequent partial or complete closure of the transport paths.
12. No solubility effect is included.
13. The effect of LiOT precipitation which can be important at low temperatures, in particular for Li_2O, is not included.
14. The available data are not sufficient to describe the kinetics of the chemical reactions occurring in the purge. Therefore, the approach used to model purge chemistry is to assume that the kinetics of the relevant chemical reactions occur fast enough so that local chemical equilibrium in the pore is always maintained.

3. Numerical algorithm and code development

To make the problem amenable to analysis, an efficient method of solution is needed to solve the system of governing differential equations and associated boundary conditions. In general, few of the analyses are exact in the sense that mathematical approximations are required in solving the equations represented in the model. Analytic solutions of the problem are usually restricted to relatively simple, idealized geometries and

boundary conditions, and the corresponding results may not be fully applicable in realistic situations. In particular, tritium transport in a ceramic media is too complex for analytic treatment and numerical solutions of the governing partial differential equations are required. However, this need no longer presents a barrier to implementation of a model with the extensive libraries of computer code packages now available. A unique method does not exist a priori and an enormous variety of numerical techniques, with intrinsic advantages and disadvantages, are available. A compromise between accuracy in the prediction and computational time required for the execution must often be reached. In particular, in transient analysis, and especially for problems involving systems of stiff ordinary differential equations (rate equations), the use of very small time-steps to advance the solution may degrade the calculation execution efficiency and considerably increase the need of high CPU times. For numerical algorithms based on finite-difference schemes the accuracy of the algorithm and the required computational time strongly depend on the number of spatial nodes and the discretization error is limited by choosing sufficiently small time-steps.

3.1. Dimensionless form of the governing equations

A nondimensional formulation of the equations and associated boundary conditions outlined in the previous section is hereafter described. The nondimensional positions within the model are defined as follows:

$$\eta = r/r_g, \tag{51}$$

$$\xi = x/x_{gb}, \tag{52}$$

$$\zeta = z/z_{ip}. \tag{53}$$

The grain diffusion time constant is used for nondimensionalizing the time. It is defined as:

$$\psi_t = r_g^2/D_{g_{min}}. \tag{54}$$

The nondimensional time may then be expressed as:

$$\tau = t/\psi_t. \tag{55}$$

The nondimensional tritium production rate is defined as:

$$\tilde{\mathcal{G}} = \mathcal{G}/\mathcal{G}_{max}. \tag{56}$$

The nondimensional tritium concentrations are defined for the grain and grain boundary regions respectively as:

$$u = C_g/\omega_g, \tag{57}$$

$$w = C_{gb}/\omega_{gb}. \tag{58}$$

The nondimensional concentrations of species (i) in the interconnected pore system are defined as:

$$v^{(i)} = C_p^{(i)}/\omega_{ip}. \tag{59}$$

where the following normalization factors for the concentrations calculated in the different regions of the model are defined as:

$$\omega_g = \psi_t \mathcal{G}_{max}, \tag{60}$$

$$\omega_{gb} = \psi_t \frac{V_g}{V_{gbg}} \mathcal{G}_{max}, \tag{61}$$

$$\omega_{ip} = \psi_t \frac{N_{gip} V_g}{V_{ip}} \mathcal{G}_{max}/2. \tag{62}$$

Eqs. (13) and (17) then become:

$$\frac{\partial u(\eta, \tau)}{\partial \tau} = \frac{D_g(T)}{D_{g_{min}}} \left[\frac{\partial^2 u(\eta, \tau)}{\partial \eta^2} + \frac{2}{\eta} \frac{\partial u(\eta, \tau)}{\partial \eta} \right] + \tilde{\mathcal{G}}(\tau), \tag{63}$$

and

$$\frac{\partial w(\xi, \tau)}{\partial \tau} = \left(\frac{D_{gb}(T)}{D_{g_{min}}} \frac{r_g^2}{x_{gb}^2} \right) \left[\frac{\partial^2 w(\xi, \tau)}{\partial \xi^2} \right]. \tag{64}$$

In order to consistently solve the system of rate equations governing the dynamics of the adsorbed species on the breeder surface, one has to couple at each pore increment $\Delta\zeta$ and time-step $\Delta\tau$ the processes of adsorption from the bulk and from the pore and desorption into the pore.

In general, the concentration of each species (i) in the interconnected pore system is affected by three different simultaneous processes: (1) diffusion through the pore, (2) adsorption/desorption at the surface (phase boundary) and (3) reactions in the gas phase.

This initial version of the model MISTRAL assumes that the hydrogen isotopes in the pore are either completely in their reduced states or completely in their oxidized states. Thus, in the following equations the index (i) could refer to species HT, T_2 or H_2 in the former case, or to species HTO, T_2O and H_2O in the latter case. The index (j) refers to the individual H and T atoms, irrespective of their chemical states.

An effective nondimensional concentration within the pore, at each nodal point k and at each instant n for each gas species (j) can be expressed as follows:

$$v_{eff_{k,n+1}}^{(j)} = \sum_{(i)} \gamma_{(i)}^{(j)} \left(\frac{v_{k,n}^{(i)}}{\sqrt{M^{(i)}}} \right) - \left(\theta_{k,n+1}^{(j)} - \theta_{k,n}^{(j)} \right) \frac{\omega_t}{\omega_{ip}}, \tag{65}$$

where the summation includes all the gas species (i) in the pore and the term $\gamma_{(i)}^{(j)}$ represents the number of atoms of species (j) per molecule of species (i). The minus sign in the second term of eq. (65) accounts for the fact that for $\theta_{k,n+1}^{(j)} \le \theta_{k,n}^{(j)}$ there is a depletion of coverage on the surface (i.e., release of gas from the surface to the pore system).

The system of rate equations in nondimensional form to be solved for the coverage of species (j) at each nodal points, k, is then:

$$\frac{d\theta_{k,n+1}^{(j)}}{d\tau} = \Re_{ads}(T)\left[\sum_{(i)}\gamma_{(i)}^{(j)}\left(\frac{v_{k,n}^{(i)}}{\sqrt{M^{(i)}}}\right) - \left(\theta_{k,n+1}^{(j)} - \theta_{k,n}^{(j)}\right)\frac{\omega_1}{\omega_{ip}}\right](1-\theta_{k,n+1})^2 - \Re_{des}(T)\theta_{k,n+1}^{(j)}\theta_{k,n+1} + \Re_{beta}(T)w_{k,n+1}(1,\tau)(1-\theta_{k,n+1}), \quad (66)$$

where:

$$\Re_{ads}(T) = \frac{\sigma N_z}{\sqrt{8\times 10^{-3}\pi}}\sqrt{RT}\,\frac{\omega_{ip}}{N_S}\psi_t \times \exp\left(-\frac{E_{ads}(T,\theta)}{RT}\right), \quad (67)$$

$$\Re_{des}(T) = 2\left(\frac{RT}{N_{avo}\,h}\right)\psi_t\,\exp\left(-\frac{E_{des}(T,\theta)}{RT}\right), \quad (68)$$

$$\Re_{beta}(T) = \beta_0\left(\frac{A_{gb}\cdot N_{gbg}}{S_{BET}\rho V_g}\right)\frac{\omega_{gb}\psi_t}{N_S}\exp\left(-\frac{E_{des}(T,\theta)}{RT}\right). \quad (69)$$

The last term on the right-hand-side of eq. (66) is $\neq 0$ only for (j) = T (tritium). All the symbols used have been explained in the previous section and have been summarized in the nomenclature section at the end of this paper.

At each time-step $\Delta\tau$ the solution of the system of rate equations provides at each nodal point through the pore k the new values $\theta_{k,n+1}^{(j)}$ of the coverage for the adsorbed species (j).

The system of eqs. (31) describing diffusion of species (i) along the interconnected pore system becomes:

$$\frac{\partial v^{(i)}(\zeta,\tau)}{\partial\tau} = \frac{r_g^2}{z_{ip}^2}\frac{\partial}{\partial\zeta}\left[\frac{D_{P_{eff}}^{(i)}(T)}{D_{g_{min}}}\frac{\partial v^{(i)}(\zeta,\tau)}{\partial\zeta}\right] + \bar{\mathcal{G}}_p^{(i)}(\zeta,\tau), \quad (70)$$

where $\bar{\mathcal{G}}_p^{(i)}(\zeta,\tau)$ is the nondimensional source/sink term in the pore defined in eq. (40) for the gas species (i) and is evaluated as the net flux of molecules of species (i) into the pore (i.e., desorption minus adsorption fluxes).

In terms of nondimensional variables the source/sink term for the species (i) at each nodal point k through the interconnected pore system and instant n is:

$$\bar{\mathcal{G}}_{P_{k,n+1}}^{(i)} = 2\left[k_{des}(T,\theta)\theta_{k,n+1}^{(j)}\cdot\theta_{k,n+1} - k_{ads}^{(i)}(T,\theta)\omega_{ip}v_{k,n+1}^{(i)}(1-\theta_{k,n})^2\right]\omega_1. \quad (71)$$

An iterative-type numerical procedure is required to advance the solution for the coverages of each species (j) adsorbed onto the surface and for the concentrations of species (i) into the pore. In order to decouple at each pore-increment and time-step the solution into the pore from that at the phase boundary and to avoid a lengthy iterative scheme, the following expression for $\bar{\mathcal{G}}_p^{(i)}$ is proposed in eq. (70) at each nodal point k and time n:

$$\bar{\mathcal{G}}_{P_{k,n+1}}^{(i)} = \gamma_{(j)}^{(i)}\left[\frac{\theta_{k,n+1}^{(j)} - \theta_{k,n}^{(j)}}{\Delta\tau}\right] + \left[\bar{\mathcal{G}}_n - \left(\frac{\bar{I}_{g_{k,n+1}} - \bar{I}_{g_{k,n}}}{\Delta\tau}\right) - \left(\frac{\bar{I}_{gb_{k,n+1}} - \bar{I}_{gb_{k,n}}}{\Delta\tau}\right)\right], \quad (72)$$

where $\gamma_{(j)}^{(i)}$ represents the number of molecules of species (i) per atom of species (j). The terms in the second parenthesis represent tritium production, changes of the inventories in the grain and grain boundary respectively, and they differ from zero only if (i) represents a tritium-bearing species.

Finally, eqs. (43) and (44) expressing chemical equilibrium among the diffusing gas species in the pore become:

$$\frac{\left[v^{(HT-X)}\right]^2}{v^{(T_2-X)}v^{(H_2-X)}} = \begin{cases} K_{eq}(1) \text{ for reduced states,} & (73)\\ K_{eq}(2) \text{ for oxidized states,} & (74)\end{cases}$$

where in the reduced state X vanishes and in the oxidized state X represents oxygen. The conservation of total number of atoms for each hydrogenic species before and after the reaction in the gas phase yields to:

$$\text{hydrogen atoms} \Rightarrow \left[2v^{(H_2-X)} + v^{(HT-X)}\right]_{before} = \left[2v^{(H_2-X)} + v^{(HT-X)}\right]_{after}, \quad (75)$$

$$\text{tritium atoms} \Rightarrow \left[2v^{(T_2-X)} + v^{(HT-X)}\right]_{before} = \left[2v^{(T_2-X)} + v^{(HT-X)}\right]_{after}. \quad (76)$$

The boundary and interface conditions in terms of the nondimensional variables become:

– *for the grain region*:

$$u(1,\tau) = w(0,\tau), \quad (77)$$

$$\left(\frac{\partial u(\eta,\tau)}{\partial\eta}\right)_{\eta=0} = 0, \quad (78)$$

– *for the grain boundary region*:

$$\frac{4\pi r_g^2 N_{ggb}}{r_g}\left[\frac{\partial u(\eta,\tau)}{\partial \eta}\right]_{\eta=1} = \frac{A_{gb}D_{gb}}{x_{gb}V_{gbg}}\left[\frac{\partial w(\xi,\tau)}{\partial \xi}\right]_{\xi=0}, \tag{79}$$

$$\frac{D_{gb}}{x_{gb}}\left[\frac{\partial w(\xi,\tau)}{\partial \xi}\right]_{\xi=1} = \beta_0 w(1,\tau)(1-\theta)\exp(-E_\beta/RT), \tag{80}$$

– *for the interconnected pore region*:

$$\left(\frac{\partial v^{(i)}(\zeta,\tau)}{\partial \zeta}\right)_{\zeta=0} = 0, \tag{81}$$

$$v^{(i)}(1,\tau) = C^{(i)}_{purge}/\omega_{ip}. \tag{82}$$

The nondimensional forms of the tritium inventory components given in eqs. (47) through (49) to be evaluated for the grain, grain boundary and surface at each nodal point k through the pore and instant n are defined as:

– *Tritium inventory in one grain*:

$$\tilde{I}_{g_n} = u_{1,n}\left[\frac{\Delta\eta}{2}\right]^3 + u_{n_{r_g},n}\left[1-\left(1-\frac{\Delta\eta}{2}\right)^3\right] + \sum_{m=2}^{n_{r_g}-1} u_{(m,n}\left[\left(\eta(m)+\frac{\Delta\eta}{2}\right)^3 - \left(\eta(m)-\frac{\Delta\eta}{2}\right)^3\right]. \tag{83}$$

– *Tritium inventory in the grain boundary (normalized to one grain)*:

$$\tilde{I}_{gb_n} = w_{1,n}\frac{\Delta\xi}{2} + w_{n_{x_{gb}},n}\frac{\Delta\xi}{2} + \sum_{m=2}^{n_{x_{gb}}-1} w_{m,n}\Delta\xi. \tag{84}$$

– *Tritium inventory on the surface (normalized to one grain)*:

$$\tilde{I}_{surf_n} = \frac{S_{BET}\rho N_S \theta^T_{k,n}}{\omega_g}. \tag{85}$$

The nondimensional forms of the tritium inventory in the pore, given in eq. (50), is at each instant n:

– *Tritium inventory in the interconnected pore (normalized to one grain)*:

$$\tilde{I}_{ip_n} = \sum_{\substack{\text{T containing}\\ \text{species } (i)}} \gamma^{(T)}_{(i)}\frac{1}{N_{gip}} \times\left[v^{(i)}_{1,n}\frac{\Delta\zeta}{2} + v^{(i)}_{n_{x_{ip}},n}\frac{\Delta\zeta}{2} + \sum_{m=2}^{n_{x_{ip}}-1} v^{(i)}_{m,n}\Delta\zeta\right]. \tag{86}$$

In eq. (86), $\gamma^{(T)}_{(i)}$ represents the number of tritium atoms per molecule of tritium-bearing species (i).

3.2. Initial conditions

The evaluation of the initial conditions is required to start the transient calculations and to advance the solution. Two cases are in general possible: (1) reactor start-up, and (2) steady-state. In the case of reactor start-up, at $t = 0$ there is no tritium generation in the system and therefore the concentrations of tritium in the grain, grain boundary, surface and pore regions are equal to zero. Hydrogen may be added to the purge before or after reactor start-up. In the latter case, no hydrogen is present in the system at $t = 0$. In the former case, the initial value of the nondimensional concentration of H_2 at the mouth of the interconnected pore is given by:

$$v^{(H_2)}(1,0) = C^{(H_2)}_{purge}/\omega_{ip}, \tag{87}$$

and its distribution along the pore is obtained by solving eq. (70) at steady-state. The value of the hydrogen coverage is obtained by solving eq. (66) for $(j) = H$ at steady-state, which is not linear in $\theta^{(H)}$, by using an iterative scheme.

In the condition of initial steady-state, to calculate the initial concentrations of gas species included in the model, the system of eqs. (63), (64), (66) and (70) and corresponding boundary conditions has to be solved by setting the left-hand-side terms equal to zero. In particular, at steady-state, the source term given by eq. (72) for the diffusion equation governing the concentrations in the interconnected pore reduces to the tritium generation in the bulk in the case of tritium-bearing species and vanishes for species not containing tritium. Besides, the concentrations of gas species in the pore must satisfy also the equilibrium relationships (73), (74), (75) and (76).

The final concentrations of gas species present in the pore are at this point fully characterized, and so is the flux of tritium atoms at the solid/gas interface. The system of nonlinear algebraic equations obtained by setting equal to zero the left-hand-side term in eq. (66) is solved. The process is iterative and consists of solving for the value of the coverages, using an attempted value for the coverage to determine the corresponding activation energy for adsorption and desorption. The process is repeated until convergence is reached between the attempted value and the calculated one, and it is carried out at each pore-increment.

For the steady-state evaluation of the tritium concentration in the effective bulk, just beneath the surface,

the boundary condition shown in eq. (80) is modified as follows:

$$\beta_0 w(1,0)(1-\theta)\exp(-E_\beta/RT)\omega_{gb}A_{gb}N_{gbg} = V_g\mathscr{G}(0), \quad (88)$$

which may be solved for the tritium concentration in the grain boundary $w(1, 0)$. Finally, the steady-diffusion equations in the grain and grain boundary regions, obtained by setting equal to zero the left-hand-side term of eqs. (63) and (64), are solved in series by using the boundary conditions given in eqs. (77), (78), (79) and (80). The process is carried out for each pore-increment.

3.3. Calculational procedure

The proposed numerical algorithm is based on a finite-difference scheme whose accuracy and required computational time depend on the number of spatial nodes. The Crank–Nicolson [32] scheme was used because of its good stability even for large time-steps. Several numerical methods were tested to efficiently solve the system of rate equations which comes from coupling the surface region with the pore and the bulk regions. The choice and implementation of the solver formulated by Gear [33,34] has represented an important step in the development of the code. To solve at each time-step and at each spacial node the coupled set of time-dependent nonlinear partial differential equations describing the transport processes, the choice of an overall integration scheme, which couples all the regions of the model, requires an iterative type numerical procedure, which often needs long running times consistent with the required accuracy of the predictions. In order to avoid a lengthy iterative scheme to advance the solution in each region of the model, the integration procedure has been consistently decoupled for each model zone by defining adequate interfacial assumptions for the different regions of the model, as indicated hereafter. The calculations are carried out for the grain and grain boundary regions first, followed by the surface region and finally for the interconnected pore system. The evaluation of the initial conditions is required to start the transient calculations and to advance the solution, and the initial values for the concentrations for all the species included in the model are evaluated as described in section 3.2.

The solution procedure consists of first solving the grain and grain boundary regions in series, for each pore length increment $\Delta\xi$, by defining the proposed boundary and initial conditions. The value of the coverage from the previous time-step is used to evaluate the boundary condition shown in eq. (80) and the values of the tritium concentrations in the grain and grain boundary, $u(\eta, \tau)$ and $w(\xi, \tau)$ respectively, are evaluated for the next step for the grain and grain boundary nodes. This assumption is reasonable because in the range of temperatures of interest, θ tends to be small and for the very small time-steps used in the computations change in the term $(1-\theta)$ from one time-step to another would have a negligible effect on eq. (80).

The system of rate equations governing the dynamics of the adsorbing and desorbing species included in the model is then solved for the pore nodes considering the fluxes into and from the surface, whose magnitudes vary through the pore length. In this regard, the incoming flux from the bulk that goes onto the surface is fully characterized by the value of the tritium concentration in the effective bulk just beneath the phase boundary $w(1, \tau)$ at a certain pore-increment, and the total coverage at the previous time-step $\theta_{k,n}$. The adsorption and desorption fluxes from and to the interconnected pore system are fully characterized in terms of the effective pore concentrations for the species (i) given in eq. (65), which include the values of the pore concentrations at the previous time-step and the change in coverage which occurs in the interval $\Delta\tau$. Because of the dependence of the heat of adsorption on the degree of coverage, the system of rate equations is clearly nonlinear. However, for ease of calculation and based on the fact that changes in θ from one time-step to another tend to be very small, the value of the total coverage at the previous time-step has been used to evaluate the corresponding value of activation energy for desorption. The system of rate equations is then solved to evaluate at each pore-increment, and for each gas species, the new values of the coverages at each time-step. The next computational step consists of solving the diffusion eq. (70) for each gas species (i) included in the model through the network of interconnected pores. The coupling between the surface-bulk system and the pore region is represented by the source/sink term $\tilde{\mathscr{G}}_p^{(i)}$ which is characterized by eq. (72). Finally, the effect of reactions in the gas phase is included by solving at each pore-increment eqs. (73), (74), (75) and (76). The final values of the concentration in the pore region are then determined along with the release of tritium from the end of the interconnected pores, which is expressed in terms of the gradient of the concentration of tritium-bearing species, as shown in eq. (46).

3.4. Code accuracy and convergence

The modeling of tritium transport and release in solid breeders is based on the integration of a system of

continuity equations of mass. Therefore, it is particularly important to account how well mass is conserved (including mass transport across the system boundaries) through the course of the calculations. For this reason, the concentrations of species in each morphological region of the breeder (i.e., within the breeder grains, the grain boundaries, the surfaces and the pores) are of interest in gas release studies. In this respect, in the code MISTRAL, an accurate control is carried out at each time-step to verify that the mass balance within the different breeder regions is maintained. $\mathscr{R}_n(t)$ represents the normalized tritium release as function of time, so that $f(t) = 1 - \mathscr{R}_n(t)$ is the fraction retained in the ceramic at time t. While the time-dependent concentration results are useful, it is nonetheless difficult to visualize and assess the accuracy of the results based on the concentrations alone. Therefore, an important indication of the code accuracy and stability comes from the fact that at steady-state the condition $\mathscr{R}_n(t) = 1$ has to be satisfied. Besides, this value has to be kept through the evolution of the calculations if nothing in the system is changed. When a variation is induced, the values of key quantities such as concentrations, coverages, inventories and release change, but, after sufficiently long times, the release has to reach the steady-state condition again of $\mathscr{R}_n(t) = 1$.

As a compromise between the accuracy of the results and the computational time required for the analyses, the following numbers of nodal points in the different regions were chosen to carry out the calculations: grain: 10; grain boundary: 10; and pore: 20.

4. Description of the model capabilities and results of the calculations

The tritium transport model MISTRAL has options which allow the handling of complicated transient conditions, which are often representative of typical in-pile tritium experiment conditions and which are all expected to occur during the operation of a solid breeder blanket in an experimental or commercial fusion reactor. In particular, the model can analyze temperature, purge gas composition and tritium generation rate transients and any combination of these.

The calculation of the space and time evolutions of the tritium and tritium-bearing species concentrations in the different phases, as well as the kinetics of the release, requires the introduction of specific input data to specify the state of the considered candidate breeder materials together with the operating conditions, namely, tritium generation rate, temperature distribution, purge gas composition and their time-dependent evolutions. The as-fabricated state of the material is generally described by defining the pellet or specimen geometry, the average grain radius, the specific breeder surface area (BET), the density, the breeder porosity and the tortuosity of the pores. All the other geometrical quantities

Table 1
Properties data and parameters used for the analysis

Material	$LiAlO_2$	Li_4SiO_4
Tritium generation rate, $\mathscr{G}$ (10^{19} atoms/m^3 s)	0.55	4.32
Average grain radius, r_g (10^{-6} m)	0.5–1	13
Density (TD), ρ (kg/m^3)	2610	2390
Porosity, ϵ_p	0.19	0.20
Tortuosity, δ	$1/\epsilon_p$	$1/\epsilon_p$
Pore diffusion factor, f_{DP}	0.04	0.04
BET area, S_{BET} (m^2/kg)	700	770
Breeder volume, V (m^3)	1.5×10^{-6}	3.64
Purge flow composition	He + 0.1–0.01–0.001% H_2	He + 1% H_2
Grain diffusion pre-exponential factor, D_{g0} (m^2/s)	1.99×10^{-9} [42]	2.1×10^{-11} [42]
Grain diffusion activation energy, E_g (kJ/mol)	90.4 [42]	64 [42]
Bulk adsorption pre-exponential factor, β_0 (m/s)	$1\times10^{13}/\sqrt{N_S}$ [19]	$1\times10^{13}/\sqrt{N_S}$ [19]
Bulk adsorption activation energy, E_β (kJ/mol)	10 (parameter)	10 (parameter)
Adsorption activation energy, E_{ads} (kJ/mol)	20	20
Heat of adsorption as a function of θ, $Q(\theta)$ (kJ/mol)	(Fischer's data) [38] (at about 600 °C)	(Fischer's data) [38] (at about 600 °C)
Desorption activation energy, $E_{des}(\theta)$ (kJ/mol)	$E_{ads} + Q(\theta)$	$E_{ads} + Q(\theta)$

relevant for the calculations are intrinsically evaluated in the code. The purge flow condition is described in terms of its partial pressure and chemical composition, and its evolution during the purge gas composition transient.

In order to assess the applicability and flexibility of the model, several examples were analyzed for candidate fusion blanket ceramics such as $LiAlO_2$ and Li_4SiO_4, whose properties are summarized in table 1. The results of the analysis are hereafter presented and discussed. The comparison of model predictions with results available from in-pile tritium recovery experiments, carried out to assess the adequacy of this tritium transport model, is presented in Part II of this paper [6].

4.1. Transient tritium release behavior after a temperature change

Modeling studies on the behavior of tritium release and surface coverages during temperature transients using the proposed MISTRAL model for lithium metasilicate (Li_2SiO_3) are presented by the authors in ref. [35]. Here, as an example of applicability of the model for a case of temperature transient, the analysis of the release behavior after an increase in temperature is presented for the $LiAlO_2$ samples irradiated in the MOZART experiment purged with helium containing protium. The properties and parameters used for this case are summarized in table 1. During the temperature transient the gas composition and the tritium generation rate were unchanged and kept to He + 0.01% H_2 and 5.5×10^{18} atoms/m^3 s, respectively. Fig. 4 shows the tritium release rate which has been normalized to the tritium generation rate for this specific case. To illustrate the effect of the pore diffusivity, curves for three effective pore diffusion coefficients are shown:

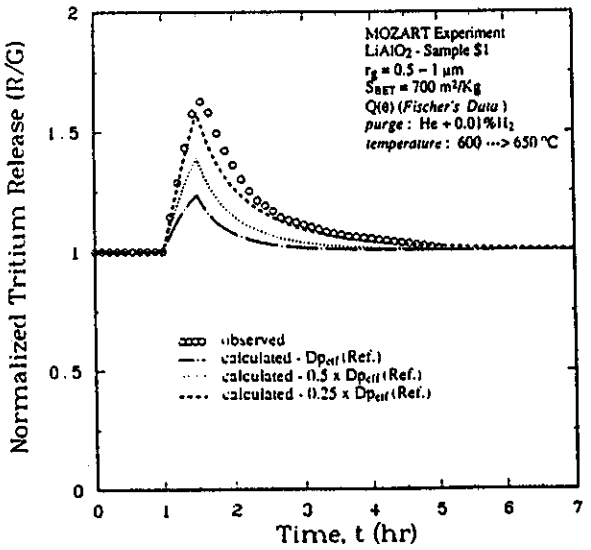

Fig. 4. Calculated and observed tritium release after a temperature increase at constant purge composition for the aluminate sample S1 irradiated in the MOZART experiment (run 3.6).

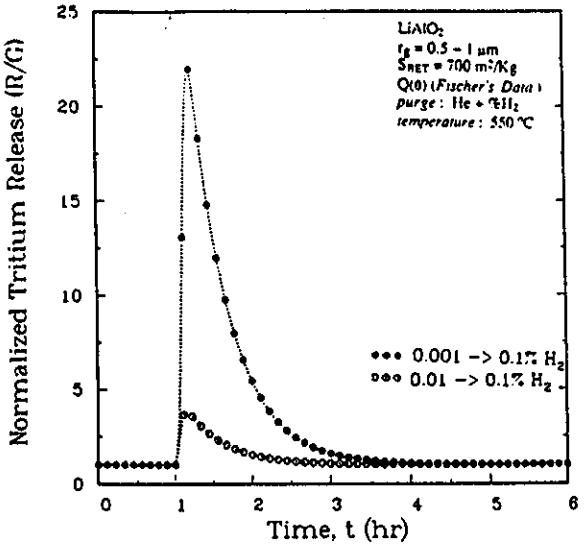

Fig. 5. Effect of changes in purge gas composition on the tritium release.

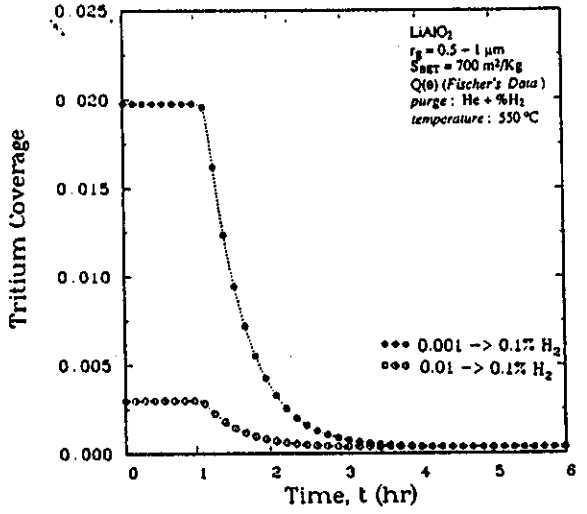

Fig. 6. Effect of changes in purge gas composition on tritium coverage at a pore location $z = 0.25 z_{ip}$.

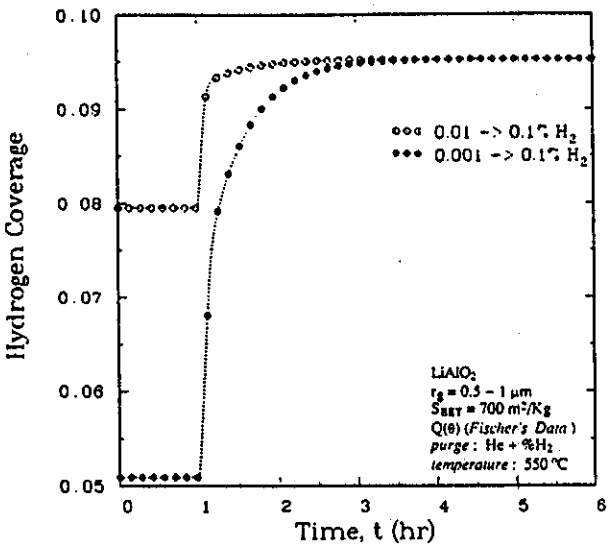

Fig. 7. Effect of changes in purge gas composition on hydrogen coverage at a pore location $z = 0.25z_{ip}$.

$D_{p_{eff}}$(ref.) ($= f_{DP}D_p$), $0.5D_{p_{eff}}$(ref.) and $0.25D_{p_{eff}}$(ref.). Pore diffusion can be seen to be quite important in controlling the peak and slope of the release curve following the transient. For comparison, the normalized observed release profile is also indicated. The model predictions agree best with the measured profile for the case of $0.25D_{p_{eff}}$(ref.).

4.2. Transient tritium release behavior after a change in purge gas composition

Several recent in-pile tritium extraction experiments such as TRIO [28], MOZART [29] and VOM-23 [30] have shown that the tritium release and the inventory are strongly affected by a change in purge gas composition. In particular, addition of small quantities of hydrogen to the helium purge (up to about 1% by volume of hydrogen) was found to substantially enhance the tritium release by effectively causing a reduction in the tritium surface coverage and inventory. It becomes then crucial for a model to have the capability to fully characterize the effect of changes in purge gas composition, and, in particular, to include different gas species and to attempt the description of competitive simultaneous effects that occur in the pore and phase boundary regions.

As a typical example selected to test the applicability of the MISTRAL model for the case of a change in purge gas composition, the analysis of a $LiAlO_2$ sample, with the same material properties as summarized in table 1, has been carried out. Two cases have been analyzed where the purge gas mixtures of He + 0.01% H_2 and He + 0.001% H_2, respectively, were replaced by the gas mixture He + 0.1% H_2. The reactor power (i.e. the tritium generation rate) was unchanged as was the temperature which was kept at 550 °C. Fig. 5 shows the tritium release profile for the two cases. Figs. 6 and 7 show the tritium and hydrogen coverages respectively. The analysis indicates that the increase of hydrogen (protium) in the purge results in a build-up of hydrogen partial pressure in the network of pores, which increases the adsorption fluxes of hydrogen-bearing species on the surface and therefore the hydrogen coverage. Hydrogen basically swamps the surface and replaces the tritium adsorbed there, which therefore desorbs to the pore and diffuses out of the pore to the purge. A clear indication of the swamping effect which occurs at the breeder surface along the network of pores is shown in figs. 8 through 10, which show the coverages and the

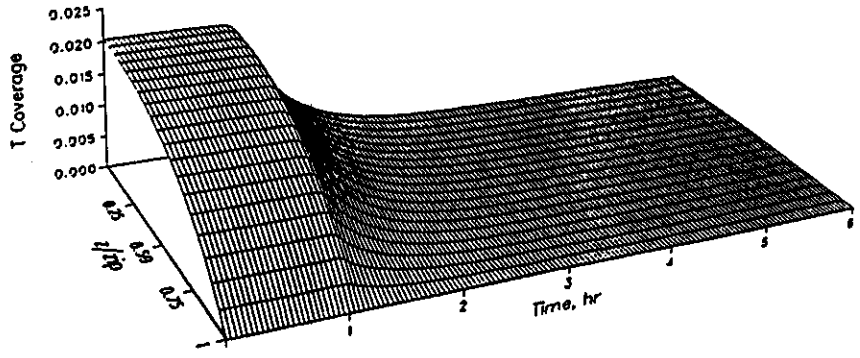

Fig. 8. Predicted tritium coverage distribution through the interconnected pore during assumed purge transient ($T = 550$ °C; purge change = He + 0.001% H_2 → He + 0.1% H_2).

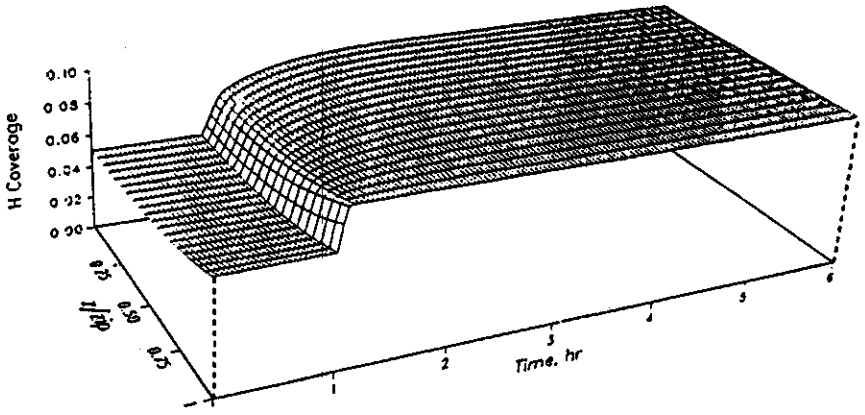

Fig. 9. Predicted hydrogen coverage distribution through the interconnected pore during assumed purge transient ($T = 550\,^{\circ}C$; purge change = He + 0.001% H_2 → He + 0.1% H_2).

HT concentration through the interconnected pore system for the case of a purge transient from He + 0.001% to He + 0.1%. In the figures z/z_{ip} represents the effective nondimensional pore length ($z = 0$ is the beginning of the interconnected pore, $z = z_{ip}$ is the end or mouth of the interconnected pore system).

4.3. Transient tritium release behavior after a reactor power change

The model can be applied to investigate cases of change in reactor power (i.e. tritium generation rate). For this particular case, the water-cooled solid breeder blanket design proposed by Gohar et al. [36] for the International Thermonuclear Experimental Reactor (ITER) was analyzed. This example has been chosen because cyclic operation, which is anticipated for ITER, creates a very complex situation for the prediction of the tritium release behavior in the breeder material, which in turn is affected by the combined effect of changes in temperature and tritium generation. A more detailed description and discussion of the results of the tritium analysis carried out for a solid breeder water-cooled blanket for ITER are presented and discussed by the authors in ref. [37].

Here, results of the tritium release and inventory calculations are presented only for the solid breeder outboard region 1 of the blanket for the case of an operating scenario with 1000 s burn time and 100 s dwell time with quasi-instantaneous rise and fall. The

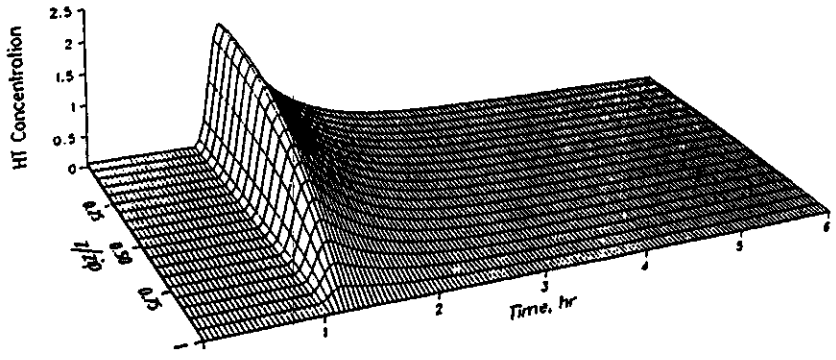

Fig. 10. Predicted (nondimensional) HT concentration distribution through the interconnected pore during assumed purge transient ($T = 550\,^{\circ}C$; purge change = He + 0.001% H_2 → He + 0.1% H_2).

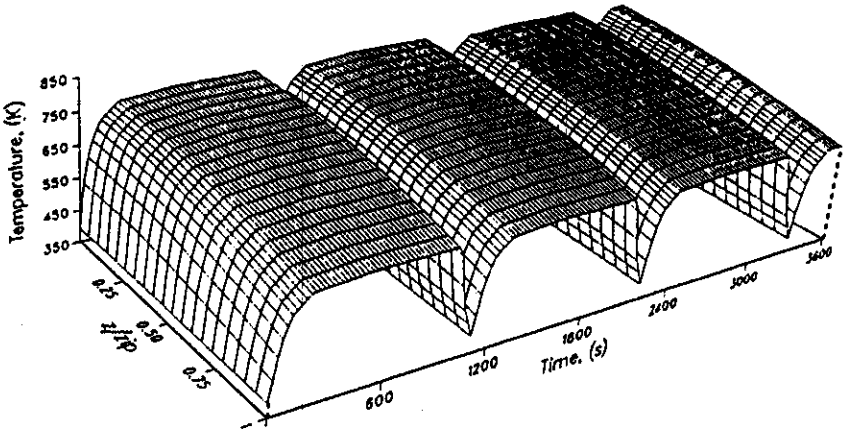

Fig. 11. Temperature distribution under pulsed operation at equilibrium in the outboard region 1 (over half the solid breeder layer thickness) of a proposed solid breeder blanket for ITER.

solid breeder material investigated was Li_4SiO_4 which, together with Li_2O, is one of the solid breeder candidates selected for the ITER design. The material properties used in the transient tritium analysis are summarized in table 1. The helium purge contained 1% H_2 and the solid breeder volume was equal to 3.64 m^3. The cyclic temperature distribution adopted for the analysis is shown in fig. 11 over half the solid breeder layer thickness and only for three operation cycles. For this case, the temperature of the solid breeder reaches thermal equilibrium during the first burn cycle at a maximum value of 775 K. It then drops to a minimum value of 392 K during the 100 s dwell time before returning to steady-state during the next burn time.

Fig. 12 indicates that the normalized tritium release is ≈ 0.95 after 10 h. Fig. 13 shows the evolution of the inventory components under pulsed operation. The total tritium inventory in the solid breeder is modeled as the

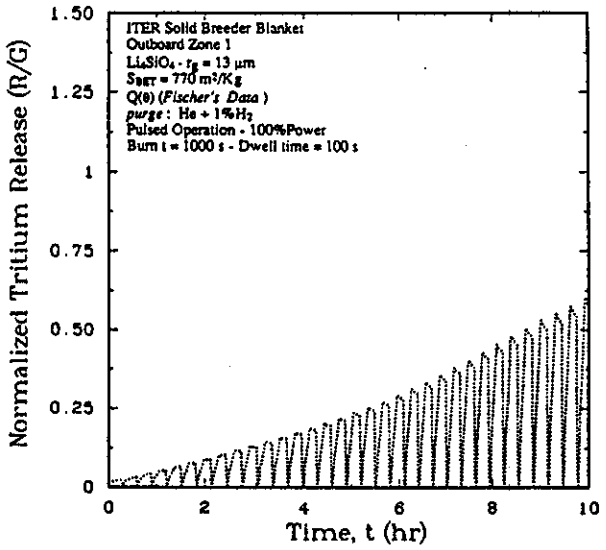

Fig. 12. Predicted tritium release in the outboard region 1 under pulsed operation (burn time = 1000 s, dwell time = 100 s) for a proposed solid breeder blanket for ITER.

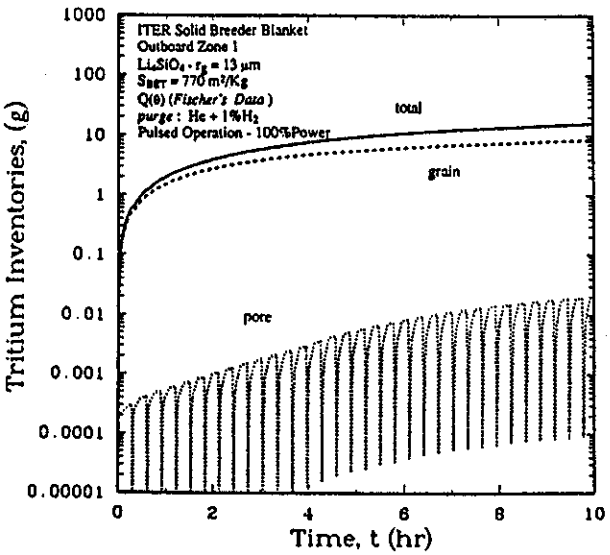

Fig. 13. Predicted transient inventories in the different regions of the blanket (burn time = 1000 s, dwell time = 100 s) for a proposed solid breeder blanket for ITER.

sum of the inventory in the effective solid (grain and grain boundary), the tritium retained on the surface and the inventory in the pore. Under the assumptions of this model, the grain boundary component is very small and almost negligible. The total tritium inventory that will be reached at steady-state is ≈ 23 g. For this case, the inventory build-up after 10 h is about half of the steady-state inventory to be attained. For the case investigated, the largest contribution to the inventory comes from the surface (i.e., in fig. 13 $I_{tot} \approx I_{surf}$).

4.4. Parametric analysis on single parameters

Modeling studies play a very important role in identifying key parameters affecting the release kinetics and the controlling processes. One way to obtain this information and therefore to gain a better understanding and insight of the investigated processes is to carry out parametric sensitivity analyses, i.e., to solve the problem for various values of the physical and chemical parameters under consideration and study the corresponding variations. A previous modeling study carried out by the authors [35] for a metasilicate sample irradiated in the LISA1 experiment, under temperature transients with a pure helium purge, clearly identified the specific surface area of the breeder (BET), the activation energy for desorption and the diffusion coefficient in the pores as important factors affecting the predictions of tritium release and concentration distributions. With the aim of showing the applicability of the model to examine the influence of several controlling parameters, an analysis has been carried out for the case of a change in purge gas composition in a lithium aluminate sample, with the same material properties as those summarized in table 1, at a constant temperature of 550 °C and at a constant tritium generation rate equal to 5.5×10^{18} atoms/m^3 s for a change in the hydrogen content of the helium purge from 0.01% H_2 to 0.1% H_2.

In particular, the effect of the following key variables on the kinetics of the release has been analyzed: (1) effect of the specific surface area of the breeder; (2) effect of the magnitude of the activation energy for desorption and its dependence on the degree of coverage; and (3) effect of the diffusion coefficient through the interconnected pore system.

Finally, an analysis of the tritium inventory build-up and release retardation which may result from radiation effects is presented for the proposed ITER solid breeder blanket of ref. [36] with Li_4SiO_4.

4.4.1. Effect of the BET area on tritium release

The analysis was carried for three values of the specific breeder surface: 350, 700 and 1500 m^2/kg. The three resulting transient release curves are compared in fig. 14 which shows that the magnitude of the peaks and the kinetics of the release are markedly affected by the value of the specific surface area. The highest and broadest peak ≈ 4.4, which occurs after a time-lag of about one hour after the change and over a time period of about 2.5 h, corresponds to the case with the largest BET area, while the lowest and narrowest peak ≈ 3.3 results for the case with the lowest value of BET area. This trend seems to be reasonable and may be justified on the grounds that the larger the BET area the larger the amount of tritium adsorbed on the surface, and, therefore, the larger will be the swamping effect whereby the adsorbed tritium is basically replaced by hydrogen and released to the pore causing a peak in the release profile.

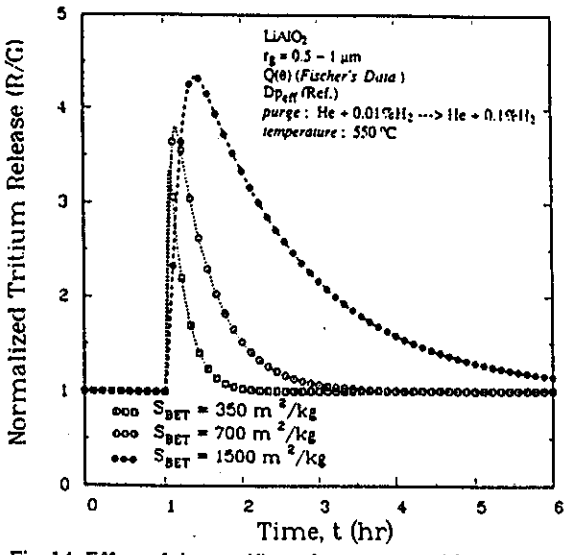

Fig. 14. Effect of the specific surface area on tritium release.

4.4.2. Effect of the heat of adsorption on tritium release

In theoretical models of tritium release from ceramic breeders, the activation energy of desorption is an important variable. Estimates of this quantity may be made from the heat of adsorption, $Q(T, \theta)$, on the basis that the activation energy of desorption is equal to the sum of the heat of adsorption and the activation energy for adsorption.

$$E_{des}(T, \theta) = E_{ads}(T, \theta) + Q(T, \theta). \quad (89)$$

Usually, the activation energy of adsorption is small so that the activation energy of desorption is usefully approximated by the heat of adsorption. It follows that

the activation energy of desorption is a function of the degree of coverage, just as the heat of adsorption is. Unfortunately, virtually no data are available for E_{des}, Q and E_{ads} as a function of θ for hydrogen or water adsorption for any lithium-base ceramic. A notable exception are the data provided by Fischer [38] for the $LiAlO_2$–$H_2O_{(g)}$ system at about 600° and which have been used in the calculations reported in this paper. The analysis has been carried out for three levels of heat of adsorption $Q(\theta)$ as a function of the coverage: (1) assuming the $Q(\theta)$ profile given by Fischer [38]; (2) $0.5Q(\theta)$; and (3) $1.2Q(\theta)$. The activation energy for adsorption was assumed constant and equal to 20 kJ/mol.

Fig. 15 shows the release profile as a function of time for the three different values of $Q(\theta)$. The analysis indicates that the magnitude of the peak of the release is significantly affected by this key parameter, being higher for the reference value of $Q(\theta)$. In the case of $1.2Q(\theta)$, the peak of the normalized release is not quasi-instantaneous but occurs after a time-lag of about one hour, and its magnitude is substantially smaller than the value for the other two cases investigated. The reason can be seen from the corresponding slopes of the tritium coverage variation with time for the three cases shown in fig. 16. The value of the tritium coverage corresponding to $0.5Q(\theta)$ is ≈ 0.0006, while for the cases with $Q(\theta)$ and $1.2Q(\theta)$ is ≈ 0.03 and ≈ 0.05, respectively. However, there is a much greater difference among the gradients

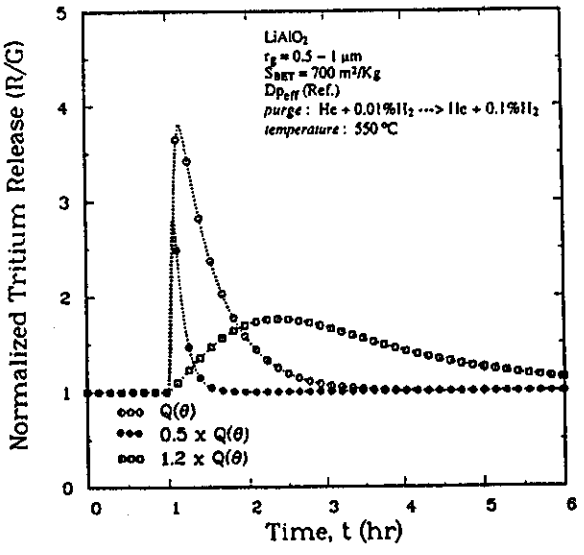

Fig. 15. Effect of the heat of adsorption on tritium release.

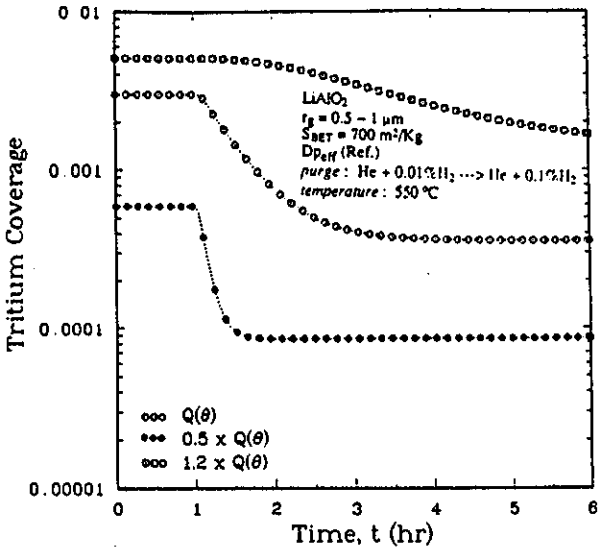

Fig. 16. Effect of the heat of adsorption on tritium coverage at a pore location $z = 0.25z_{ip}$.

following the purge composition change for the three cases, the gradient being the steepest for the lowest value of the heat of adsorption.

For purge gas composition transients in particular, the variation of the activation energy of desorption with coverage (and in effect of heat of adsorption for small activation energy of adsorption) is a key factor. It is believed that the sudden tritium release peak observed when the hydrogen content is increased can only be explained by the variation of the activation energy of desorption with θ, as can be seen from earlier modeling attempts for hydrogen purge transients presented and discussed in ref. [39]. Such a variation has been observed in metals and oxides before and can be explained in terms of surface heterogeneity and interactions between adsorbed molecules as reported by Trapnell et al. [40]. In other words, on a heterogeneous surface, there will be a tendency for the most active sites to be covered first, both because adsorption is likely to proceed more rapidly on them, and also because in a mobile layer, even if there has been random coverage initially, there will subsequently take place a spreading to the most active points. Thus, as the coverage increases, sites of lessening activity will be covered so that the heat of adsorption continuously decreases. The decrease of the heat of adsorption with increasing coverage may also be explained in terms of the forces of repulsion between molecules in the adsorbed layer. It is

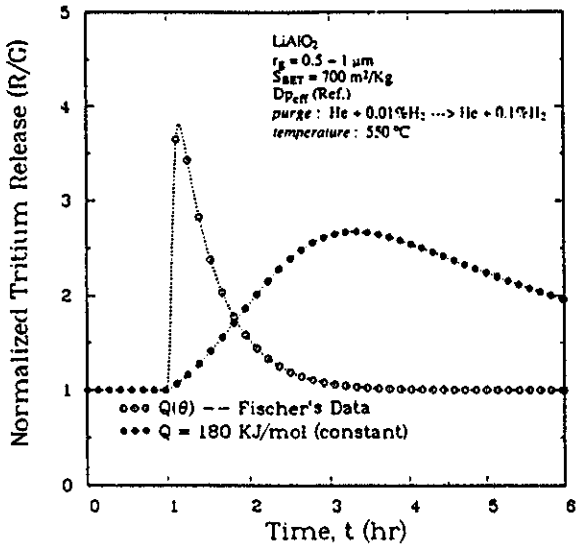

Fig. 17. Effect of the coverage dependence of the heat of adsorption on tritium release profile.

clear then that, as the coverage decreases, desorption will occur from sites of increasing activity and E_{des} continuously increases with decreasing coverage.

An example of the effect of using a constant Q as compared to a coverage-dependent one, $Q(\theta)$ is shown in fig. 17. The tritium release peak, as expected, is much sharper and closer to experimental observation for the $Q(\theta)$ case as compared to the $Q = 180$ kJ/mol case. The reason is that even a small change in θ can create a large change in the rate of adsorption/desorption because of the exponential dependence of rates of adsorption and desorption. If E_{ads} and E_{des} were constant, the only effect on the rate equations would come from the factors θ^2 and $(1-\theta)^2$ which occur over a larger characteristic time.

4.4.3. Effect of the pore diffusion coefficient on tritium release

The effect of the pore diffusion coefficient on tritium release from the MOZART $LiAlO_2$ sample following a temperature transient has been shown in fig. 4. Here the effect on tritium release following a purge transient is discussed. Three cases were examined: (1) $D_{p_{eff}}$(ref.) (i.e., $f_{DP}D_p$), (2) $0.1D_{p_{eff}}$(ref.), and (3) $0.01D_{p_{eff}}$(ref.). Cases (2) and (3) were investigated to analyze the effect of an inhibition of the diffusive step through the network of pores existing in the breeder, on the amount of gas released to the purge. This inhibition may result from phenomena such as incomplete interconnection of the pores, partial closure of the pores (which would affect the diffusion regime) caused by grain growth or sintering effect, wide distribution of pore sizes as well as from fabrication defects. Fig. 18 shows the tritium release profile for the three above cases for a change in the hydrogen content in the helium purge. A strong effect can be observed on the magnitude of the peak and on the kinetics of the release. When the effective pore diffusion coefficient is reduced by a factor of 100 the magnitude of the peak is ≈ 3.8 and is almost the same as for the case with the reference pore diffusion coefficient, but the slopes of the two release curves are significantly different, indicating for the former case a very slow return to the steady-state condition (e.g., $\mathscr{R}_n = 1$). When the effective diffusion coefficient in the pore is reduced by a factor of 10, the peak of the release increases to ≈ 4.5, but occurs after a time lag of ≈ 1–1.5 h after the change and also over a longer period. The trend of the predicted profiles may be explained on the grounds that the amount of released tritium depends strongly on the time for hydrogen to diffuse through the pore and to be adsorbed onto the breeder surface as the hydrogen partial pressure increases, but also depends on the time for the tritium-bearing species to diffuse out once they desorb from the surface. A very low diffusivity through the pore results in a build-up of tritium partial pressure in the pore and therefore to an increase of the tritium coverage.

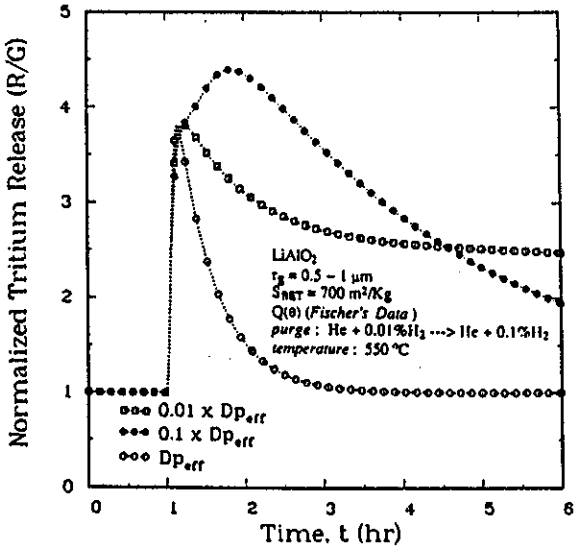

Fig. 18. Effect of the pore diffusion coefficient on tritium release.

4.4.4. Tritium release retardation and inventory build-up caused by radiation effects

It is commonly accepted that in the presence of radiation damage the gas atoms diffusing in the ceramic lattice will interact with the damage and will be temporarily retarded or trapped, as noted by MacEwan [41]. However, for a lithium-base solid breeder for fusion applications, a reliable knowledge of the field is still limited and many reaction mechanisms under irradiation conditions are not yet completely characterized. Therefore, instead of attempting a modeling approach aimed at including new phenomenological steps in the already complex tritium transport sequence, it may be useful, at this preliminary stage, to suggest a set of effective diffusion coefficients for trapping.

The reason to introduce these apparent diffusion coefficients, which would be particularly useful for parametric analyses, is to better characterize the phenomenological sequence and to evaluate the relative contribution of different release mechanisms which, under substantial radiation damage, can significantly reduce and retard the tritium release rate and, thus, increase the tritium inventory in the system. In other words, each grain of the ceramic breeder has to be treated as a homogeneous matrix with a unique diffusion coefficient, $D_{g_{trap}} \leq D_g$ describing the transport of atoms to the grain edge. In addition to radiation-induced trapping within the grains, the occurrence of restructuring, grain growth and sintering can slow down diffusion through the network of narrow interconnected pores, which provide a pathway for the release of tritium-bearing species once they have desorbed from the breeder surface, as was discussed in the previous section.

Based on this observation, a diffusion coefficient $D^{(i)}_{p_{trap}} \leq D^{(i)}_{p_{eff}}$ can be introduced to describe the effective diffusion of gas-species (i) through the pores. A parametric analysis at steady-state has been performed, for two different levels of temperature, to show the effect of varying the diffusion coefficients in the grain and pore regions of the solid breeder respectively, on the tritium inventory components.

The analysis was carried out for lithium orthosilicate (Li_4SiO_4) using the material properties and data summarized in the second column of table 1 and for a helium purge containing 1% H_2. The breeder volume of 3.64 m^3 corresponds to the outboard region 1 of the design proposed by Gohar [36].

Figs. 19 and 20 show the tritium inventory components as a function of an effective normalized grain diffusion coefficient for 250 °C and for 650 °C, respectively. $D_{g_{trap}}/D_g = 1$ represents the reference case, where

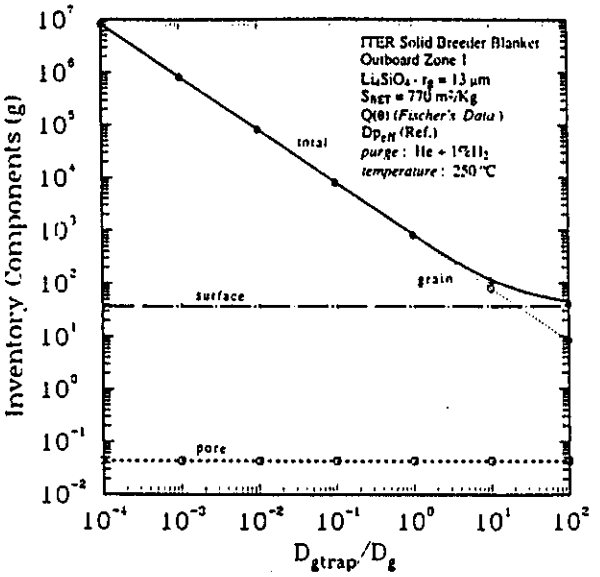

Fig. 19. Effect of the intergranular diffusion coefficient on the tritium inventory components for a proposed ITER blanket at 250 °C.

no effect of retardation of tritium diffusing through the grain is assumed. Note, however, that because of the uncertainties associated with the tritium diffusion coef-

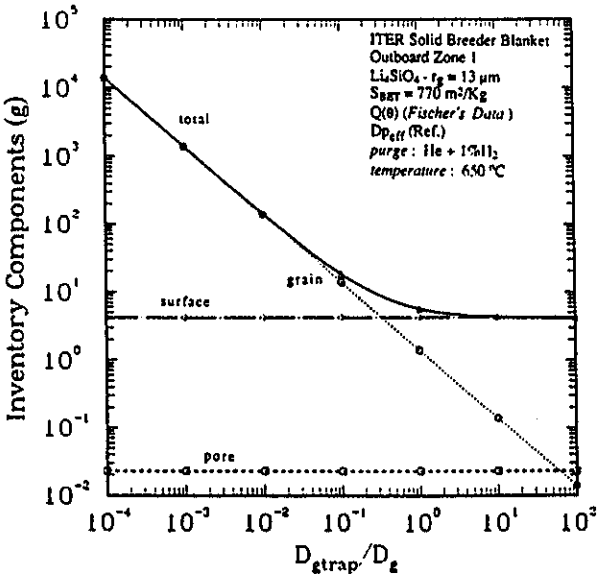

Fig. 20. Effect of the intragranular diffusion coefficient on the tritium inventory components for a proposed ITER blanket at 650 °C.

ficients in the grain, it would be more realistic to enclose the reference case within a band characterized by $D_{g_{trap}}/D_g \approx 1$. A strong dependence of the inventory in the grain, which scales as the inverse of $D_{g_{trap}}/D_g$ may be observed, while the tritium inventories on the surface and in the pore are virtually constant in each case. The inventory components depend also on the level of temperature. At 250 °C the grain component of the inventory is dominant for values of $D_{g_{trap}}/D_g \leq 20$, while for the case at 650 °C it becomes dominant only for $D_{g_{trap}}/D_g \leq 0.3$. At the reference case (i.e., $D_{g_{trap}}/D_g = 1$), the total inventory for the case at 650 °C is mostly due to tritium adsorbed at the breeder surfaces and is ≈ 7 g, while for the case at 250 °C the grain component is largely dominant and the total inventory has been evaluated to be ≈ 1000 g.

Figs. 21 and 22 show the magnitude of the tritium inventory components for different values of the effective pore diffusion coefficient for operation at 250 °C and 650 °C, respectively.

The reference condition corresponds to $D^{(i)}_{p_{trap}}/D^{(i)}_{p_{eff}} = 1$. The domain $D^{(i)}_{p_{trap}}/D^{(i)}_{p_{eff}} < 1$ portrays typical conditions of low pore diffusivity caused by factors such as incomplete interconnection of the pores and partial closure due to sintering effects. As may be observed from the analysis of the curves, a change in the pore diffusion coefficient has virtually no effect on the magnitude of the inventory in the grain, but strongly affects

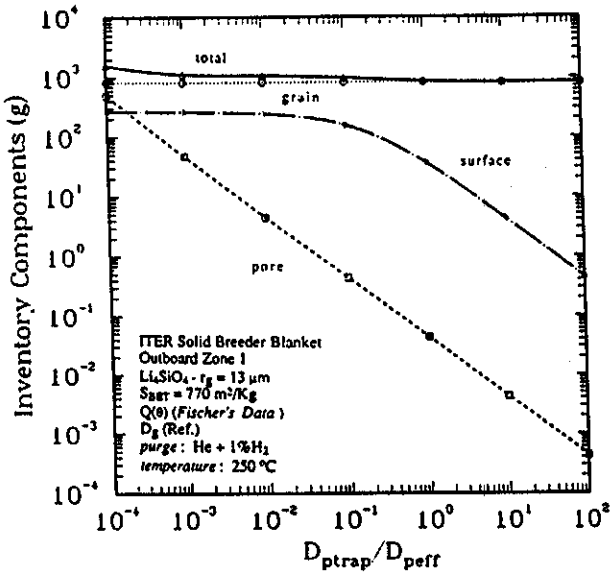

Fig. 21. Effect of the diffusion coefficient in the pore on the tritium inventory components for a proposed ITER blanket at 250 °C.

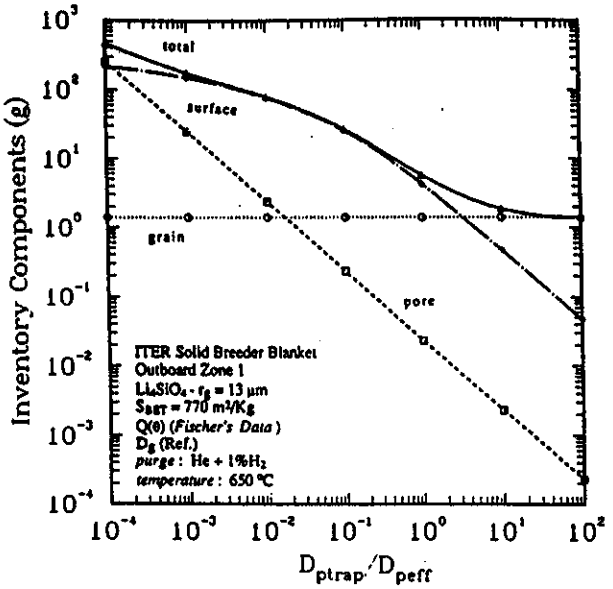

Fig. 22. Effect of the diffusion coefficient in the pore on the tritium inventory components for a proposed ITER blanket at 650 °C.

the inventory in the pore which scales as the inverse of $D^{(i)}_{p_{trap}}$, and the tritium retained on the surface that increases as $D^{(i)}_{p_{trap}}$ decreases until a saturation level is reached. This latter tritium inventory component scales as the concentration of tritium species in the pores as pore diffusion decreases and as the factor $(1-\theta)^2$, which controls the filling of adsorption sites at the surface. This factor decreases as the value of the total coverage increases to its maximum allowable value equal to $1((1-\theta)^2 \approx 0$ for $\theta \approx 1)$.

As in the previous case, the inventory components depend on the temperature level. At 250 °C, the grain component is still dominant over all the range of $D^{(i)}_{p_{trap}}/D^{(i)}_{p_{eff}}$ investigated. For the case at 650 °C, in the domain of interest (i.e., $D^{(i)}_{p_{trap}}/D^{(i)}_{p_{eff}} < 1$), the contribution of surface inventory is always dominant.

5. Summary

The tritium transport model presented in this paper builds on and substantially improves on the theoretical models on the subject already existing in the literature, in particular that of ref. [39]. It is based on a more accurate geometrical description of the breeder, and it allows for both steady-state and transient analyses. A key improvement is the simultaneous treatment of dif-

fusive processes in the bulk of the breeder and along the network of pores and surface processes at the solid/gas interface, which may all be rate controlling for tritium release. In this respect, the MISTRAL model provides an adequate selection of transport mechanisms and numerical methods, able to reproduce most of the operating conditions expected to occur in a solid breeder during irradiation in in-pile tritium recovery experiments or in an experimental or commercial fusion reactor. These operating conditions include changes in temperature, purge gas composition and reactor power. The flexibility and applicability of the model are demonstrated by application to several cases which represent typical transient conditions of interest. Other key issues relevant for tritium transport behavior addressed in conjunction with this analysis have been: (1) identification of the key parameters which may affect the release kinetics as well as the overall tritium transport behavior, such as the specific surface area of the breeder, activation energy for intragranular diffusion, activation energies for adsorption and desorption, grain size, presence of hydrogen in the purge, and the effective diffusion coefficient for tritium/hydrogen diffusion in the pore; and (2) identification of the rate-controlling step in the transport sequence leading to tritium release.

MISTRAL is particularly suitable for parametric studies and, in this regard, is of particular significance in gaining insight into the interrelationships of the various operating conditions and material properties which affect the kinetics of the release. A parametric analysis was carried out to investigate the effect of key variables, such as the BET area, the heat of adsorption and the diffusion coefficient in the pores on the tritium release. The final example studied with the aid of the model analyzes the effect of trapping of the diffusing tritium-bearing species in the grain and in the interconnected pores, which may be caused by radiation effects and which may substantially increase the fraction of tritium retained in the material. Several observations can be made as a result of the analysis. First, the breeder microstructure (e.g., BET area, grain size, porosity, pore size distribution and tortuosity) has a very strong influence on tritium transport behavior and may influence the overall kinetics of the release. For example, the effective pore diffusion can be much slower than expected, depending on the pore size distribution and degree of interconnection of the pores, and, therefore, on the fuel microstructure and on the irradiation time and temperature. Thus, it is important that the breeder microstructure be characterized before and after irradiation in particular for determining the BET area, the fraction of open porosity and pore size distribution. Second, in order to accurately calculate the tritium release from ceramic breeder materials for fusion applications, the relationship between surface coverage and adsorption and desorption activation energies must be known. Third, the strong dependence of the tritium release on variables like the BET area, the heat of adsorption (in effect the activation energy of desorption for very small activation energy for adsorption) as a function of the surface coverage, and the pore diffusion indicates the importance of accounting for the adsorption and desorption processes as a function of the local pore concentrations. This highlights the short-comings of the simpler tritium transport models developed in the past and represents a major shift in the modeling focus. Indeed, all existing models tend to oversimplify the diffusive step through the network of interconnected pores and to neglect any kind of linking between the surface and the pore regions. We believe that this coupling is crucial to correctly account for the fact that the breeder surface acts like a key interface controlling the rate of both the filling of adsorption sites from the bulk and from the pore, as well as the desorption of tritium into the pore.

The model has received extensive verification over a wide range of transient operating conditions and can be regarded as state-of-the-art based on the current level of understanding of tritium transport and release behavior in lithium-base ceramics. It must be pointed out, however, that although the model represents a major step forward in tritium modeling, there are still many areas that could be improved and in which new models could be added to develop more comprehensive predictive capabilities. Particular area of improvements for MISTRAL that should be emphasized in the future include:

- better modeling of the chemistry aspect of surface reactions;
- inclusion of oxygen in determining the pore concentrations of the different hydrogen/tritium species;
- inclusion of the effect of LiOT precipitation which is particularly important at low temperature, with emphasis on characterizing the time constants for precipitation and dissociation, and on accounting for a bulk source term;
- inclusion of a dissolution flux from the surface to the bulk;
- better characterization of radiation-induced trapping.

Nomenclature

A_{gb} transversal area for the grain boundary pathway (m^2);

$C_g(r, t)$ concentration of tritium atoms in the grain (atoms/m^3);
$C_g(r_g, t)$ concentration of tritium atoms at the edge of the grain (atoms/m^3);
$C_{gb}(x, t)$ concentration of tritium atoms in the grain boundary (atoms/m^3);
$C_{gb}(0, t)$ concentration of tritium atoms at the grain boundary/grain interface (atoms/m^3);
$C_{gb}(x_{gb}, t)$ concentration of tritium atoms in the effective bulk region just beneath the surface (atoms/m^3);
$C_p^{(i)}(z, t)$ concentration of gas species (i) in the pore (molecules/m^3);
$C_p^{(i)}(0, t)$ concentration of gas species (i) at the beginning of the interconnected pore (i.e., $z = 0$) (molecules/m^3);
$C_p^{(i)}(z_{ip}, t)$ concentration of gas species (i) at the end of the interconnected pore (i.e., $z = z_{ip}$) (molecules/m^3);
$C_{purge}^{(i)}$ concentration of gas species (i) in the purge (molecules/m^3);
D_g intragranular tritium diffusion coefficient (m^2/s);
$D_{g_{min}}$ intergranular tritium diffusion coefficient evaluated at the minimum temperature (m^2/s);
$D_{g_{trap}}$ intragranular tritium diffusion coefficient including trapping (m^2/s);
D_{g0} pre-exponential factor for intragranular diffusion (m^2/s);
D_{gb} diffusion coefficient in the grain boundary (m^2/s);
D_{gb0} pre-exponential factor for the diffusion in the grain boundary (m^2/s);
$D_K^{(i)}$ pore diffusion coefficient for species (i) for Knudsen regime (m^2/s);
$D_o^{(i)}$ pore diffusion coefficient for species (i) for ordinary regime (m^2/s);
$D_T^{(i)}$ pore diffusion coefficient for species (i) for transition regime (m^2/s);
D_p^i pore diffusion coefficient for species (i) (m^2/s);
$D_{P_{eff}}^{(i)}$ effective diffusion coefficient in the pore for species (i) (m^2/s);
$D_{P_{trap}}^{(i)}$ diffusion coefficient in the pore including trapping (m^2/s);
E_{ads} activation energy for dissociative adsorption, (J/mol);
E_β activation energy for adsorption of atoms from the bulk, (J/mol);
E_{des} activation energy for associative desorption (J/mol);
E_g activation energy for intragranular diffusion (J/mol);
E_{gb} activation energy for diffusion in the grain boundary (J/mol);
f_{DP} ratio of $D_{P_{eff}}$ to D_P;
$\mathcal{G}$ tritium production rate per unit volume (atoms/m^3 s);
$\tilde{\mathcal{G}}$ nondimensional tritium production rate;
$\mathcal{G}_{max}$ maximum tritium production rate per unit volume (atoms/m^3 s);
$\mathcal{G}_p$ effective source/sink term in the pore system (molecules/m^3 s);
$\tilde{\mathcal{G}}_p$ non-dimensional source term in the pore system;
h Planck's constant = 6.6262×10^{-34} J s;
k_B Boltzmann's constant = 1.380662×10^{-23} J/K;
$k_{ads}^{(i)}$ rate constant for adsorption of species (i) (m/s);
$k_{des}^{(i)}$ rate constant for desorption of species (i) (m^{-2} s^{-1});
k_{diss} rate constant for dissolution into bulk (s^{-1});
k_β rate constant for adsorption from the bulk (s^{-1});
i index indicating molecular gas species in the pore;
I_g tritium inventory in the grain (bulk) (g);
$\tilde{I}_g$ nondimensional tritium inventory in the grain;
I_{gb} tritium inventory component in the grain boundary (g);
$\tilde{I}_{gb}$ nondimensional tritium inventory in the grain boundary;
I_{surf} tritium retained on the breeder surface (g);
$\tilde{I}_{surf}$ nondimensional tritium inventory on the surface;
I_p tritium inventory in the pore (g);
$\tilde{I}_p$ nondimensional tritium inventory in the pore;
I_{tot} total tritium inventory (g);
$\tilde{I}_{tot}$ nondimensional total tritium inventory;
j index indicating the generic atomic species in the gas phase or at the phase boundary;
$K_{eq}(1)$ equilibrium constant for reduced hydrogen states;
$K_{eq}(2)$ equilibrium constant for oxidized hydrogen states;
L geometrical length of the pore (m);
L_e effective length for the interconnected pore system (m);
m adsorbate mass (g);

$M^{(i)}$ molecular weight of species (i) (g/mol);
N_{avo} Avogadro's number = 6.022169×10^{23} particles/mol;
N_{gbg} number of grain boundary pathways per grain;
N_{ggb} number of grains per grain boundary pathway;
N_{gip} number of grains per interconnected pore system;
N_S density of sites (in general $\approx 1 \times 10^{19}$ sites/m^2);
N_{sides} number of sides of regular polygon representing grain and pore unit cell;
N_z number of adjacent sites (in general $N_z = 4$);
p gas pressure (Pa);
Q heat of adsorption (J/mol);
R universal gas constant = 8.3144 J/mol K;
$\mathscr{R}$ tritium release rate (atoms/grain s);
$\mathscr{R}_n$ normalized tritium release;
$\Re_{ads}$ parameter for adsorption flux from the pore defined by eq. (67);
$\Re_{des}$ parameter for desorption flux to the pore defined by eq. (68);
$\Re_{beta}$ parameter for adsorption flux from the bulk defined by eq. (69);
$\Re_1^T$ flux of tritium atoms from the bulk to the surface (atoms/m^2 s);
$\Re_2(i)$ flux of molecules (i) from the pore to the surface (molecules/m^2 s);
$\Re_3(i)$ flux of molecules (i) from the surface to the pore (molecules/m^2 s);
$\Re_4(j)$ flux of atoms (j) from the surface to the bulk (atoms/m^2 s);
r radial position in the grain, (m);
r_g average grain radius (m);
r_{ip} average pore radius (m);
$s(\theta)$ sticking coefficient or probability for adsorption;
S_{BET} specific surface area of the breeder (m^2/kg);
T absolute temperature (K);
t time (s);
t_{gb} thickness of the grain boundary (m);
$u(\eta, \tau)$ nondimensional tritium concentration in the grain;
V volume of the breeder (m^3/kg);
V_g grain volume (m^3/grain);
V_{gb} volume of single grain boundary path (m^3);
V_{gbg} grain boundary volume per grain (m^3/grain);
V_{ip} volume of interconnected pore system (m^3);
$v^{(i)}(\zeta, \tau)$ nondimensional species (i) concentration in the pore;
$v_{eff}^{(i)}(\zeta, \tau)$ effective nondimensional species (i) concentration in the pore used for adsorption calculation;
$w(\xi, \tau)$ nondimensional tritium concentration in the grain boundary;
x axial position in the grain boundary (m);
x_{gb} grain boundary effective path length (m);
z axial position in the interconnected pore system (m);
z_{ip} effective length of the interconnected pore system ($z_{ip} = L_e$) (m).

Greek Letters

α_0 pre-exponential factor for dissolution into the bulk (m/s);
β_0 pre-exponential factor for adsorption from the bulk (m/s);
δ tortuosity factor;
ϵ_p porosity of the breeder;
$\gamma_{(i)}^{(j)}$ number of atoms of species (j) per gas molecule of species (i);
Γ purge flow rate (m^3/s);
η nondimensional radial position in the grain;
ψ_t time normalization constant (s);
λ mean-free-path of the diffusing species through the pore (m);
ν universal vibration frequency = $RT/N_{avo}h = k_BT/h \approx 1 \times 10^{13}$ s^{-1};
θ total coverage (fraction of adsorption sites occupied);.
$\theta^{(j)}$ coverage for the species (j) (fraction of sites occupied by atoms of species (j));
θ_0 fraction of the surface uncovered by any atom;
ρ solid theoretical density (kg/m^3);
σ condensation coefficient ($\sigma \approx 0.4$);
$\sigma_{i,l}$ constant in the Lennard–Jones potential energy function for the molecular pair (i, l);
τ nondimensional time;
ω_g normalization constant for tritium concentration in the grain (atoms/m^3);
ω_{gb} normalization constant for tritium concentration for tritium concentration in the grain boundary (atoms/m^3);
ω_{ip} normalization constant for concentration of species (i) in the pore (molecules/m^3);
$\Omega_{i,l}$ collision integral;
ξ nondimensional axial position in the grain boundary;

nondimensional axial position in the interconnected pore system.

Acknowledgements

The authors would like to thank Dr. A.K. Fischer for diligently providing the only available data for heat of adsorption as a function of the coverage for water–lithium ceramics systems. Dr. K. Fujimura for his contribution on the initial computational effort and Dr. M. Billone for his valuable input. Most of the research reported here has been carried out as part of a doctoral thesis dissertation by the first author. This work was supported by the US Department of Energy under grant #DE-FG03-86ER52123.

References

[1] D.K. Brice and B.L. Doyle, J. Nucl. Mater. 120 (1984) 230.
[2] D.L. Cummings and D.A. Blackburn, J. Nucl. Mater. 144 (1987) 81.
[3] G. Gervasini and F. Reiter, Fusion Technol. 8 (1985) 2373.
[4] J. Bénard, Adsorption on Metal Surfaces, in: Studies in Surface and Science Catalysis, Vol. 13 (Elsevier, Amsterdam, 1983).
[5] G. Federici, Ph.D. Dissertation, University of California at Los Angeles (October 1989); UCLA-FNT-30 Report (November 1989).
[6] G. Federici, A.R. Raffray and M.A. Abdou, companion paper in this volume, J. Nucl. Mater. 173 (1990) 214.
[7] J.P. Kopasz and C.E. Johnson, Progress Report on Fusion Reactor Materials. DOE/ER-0313/4 (March 1988).
[8] H. Elbel, in: Proc. 3rd Int. Conf. on Fusion Reactor Materials (ICFRM-3), Karlsruhe, Fed. Rep. Germany, October 1988, J. Nucl. Mater. 155–157 (1988) 480.
[9] A. Wheeler, Catalysis 2 (1955) 105.
[10] N. Wakao and J.M. Smith, Chem. Eng. Sci. 17 (1962) 825.
[11] G.R. Youngquist, Ind. Eng. Chem. 62-8 (1970) 52.
[12] S. Brunauer, P.H. Emmett and E. Teller, J. Am. Chem. Soc. 60 (1938) 309.
[13] J.H. Krasuk and J.M. Smith, AIChE J. 18 (1972) 506.
[14] C.N. Satterfield, Mass Transfer in Heterogeneous Catalysis (MIT Press, Cambridge, Massachusetts, 1970).
[15] R. Aris, The Mathematical Theory of Diffusion and Reaction in Permeable Catalysts, Vols. I and II (Clarendon Press, Oxford, 1975).
[16] H.S. Levine and C.J. MacCallum, J. Appl. Phys. 31 (1960) 595.
[17] M.V. Speight and J.A. Turnbull, J. Nucl. Mater. 68 (1977) 244.
[18] J.A. Turnbull and C.A. Friskney, J. Nucl. Mater. 58 (1975) 31.
[19] M.A. Pick and K. Sonnenberg, J. Nucl. Mater. 131 (1985) 208.
[20] M. Boudart and G. Djéga-Mariadassou, Kinetics of Heterogeneous Catalytic Reactions (Princeton University, Princeton, 1984).
[21] M.A. Pick and M.G. Greene, Surf. Sci. 93 (1980) L129.
[22] M.A. Pick et al., Phy. Rev. Lett. 43–44 (1979) 286.
[23] C. Wagner, Z. Phys. Chem. A159 (1932) 459; and Z. Elektrochem. 44 (1938) 507.
[24] M.I. Baskes, J. Nucl. Mater. 92 (1980) 318.
[25] P.M. Richards, J. Nucl. Mater. 152 (1988) 246.
[26] J.E. Lennard-Jones, Trans. Faraday Soc. 28 (1932) 333.
[27] R.B. Bird, W.E. Stewart and E.N. Lightfoot, Transport Phenomena (Wiley, New York, London, 1960).
[28] R.G. Clemmer et al., The TRIO Experiment Report, ANL-84-55, Argonne National Laboratory (September 1984).
[29] M. Briec, J.J. Abassin, C.E. Johnson, M. Masson, N. Roux and H. Watanabe in: Proc. 15th Symp. on Fusion Technology, Utrecht, September 1988.
[30] T. Kurasawa, H. Watanabe, E. Roth and D. Vollath, in: Proc. 3rd Int. Conf. on Fusion Reactor Materials (ICFRM-3), Karlsruhe, Fed. Rep. Germany, October 1987, J. Nucl. Mater. 155–157 (1988) 544.
[31] W.M. Jones, J. Chem. Phys. Vol. 17, No. 11 (November 1949).
[32] J. Crank and P. Nicolson, Proc. Cambridge Philos. Soc. 43 (1947) 50.
[33] A.C. Hindmarsh, GEAR: Ordinary Differential Equation System Solver Report, Lawrence Livermore Laboratory, UCID-30001, Revision 3 (December 1974).
[34] C.W. Gear, Numerical Initial Value Problems in Ordinary Differential Equations (Prentice-Hall, Englewood Cliffs, New Jersey, 1971).
[35] G. Federici, A.R. Raffray and M.A. Abdou, in: Proc. 2nd Int. Symp. on Fabrication and Properties of Lithium Ceramics (Indianapolis, 1989).
[36] Y. Gohar et al., in: Proc. 8th Topical Meeting, Salt lake City, UT, USA, Fusion Technol. 15 (1988) 864.
[37] G. Federici, A.R. Raffray and M.A. Abdou, in: Proc. 13rd Symp. on Fusion Engineering (SOFE), Knoxville, TN, October 1989.
[38] A.K. Fischer and C.E. Johnson, in: Proc. 8th Topical Meeting, Salt lake City, UT, USA, 1988, Fusion Technol. 15 (1988) 1212.
[39] A.R. Raffray, M.A. Abdou and P. Gierszewski, in: Proc. 1st Symp. on Fabrication and Properties of Lithium Ceramics, American Ceramic Society, Pittsburg, PA, USA, 1987.
[40] B.M.W. Trapnell and D.O. Hayward, Chemisorption, 2nd Ed. (Butterworths, London, 1964).
[41] J.R. MacEwan and W.H. Stevens, J. Nucl. Mater. 11 (1964) 77.
[42] K. Okuno and H. Kudo, in: Proc. 1st Int. Symp. Fusion Nuclear Technology, Tokyo, Japan, 1988, Fusion Eng. Des. 8 (1989) 355.